Biogeosciences Discuss., https://doi.org/10.5194/bg-2018-168
Manuscript under review for journal Biogeosciences
Discussion started: 14 May 2018

Biogeosciences Discussions Open Access EGU

An improved parameterization of leaf area index (LAI) seasonality in the Canadian Land Surface Scheme (CLASS) and Canadian Terrestrial Ecosystem Model (CTEM) modelling framework

[1]Ali Asaadi, [1]Vivek K. Arora, [2]Joe R. Melton, and [2]Paul Bartlett

[1]Canadian Centre for Climate Modelling and Analysis, Environment and Climate Change Canada

[2]Climate Research Division, Environment and Climate Change Canada

Corresponding author: Ali Asaadi, Canadian Centre for Climate Modelling and Analysis, Victoria, BC, V8W 2Y2, Canada

Email: ali.asaadi@canada.ca

Biogeosciences Discuss., https://doi.org/10.5194/bg-2018-168
Manuscript under review for journal Biogeosciences
Discussion started: 14 May 2018

Abstract

Leaf area index (LAI) and its seasonal dynamics are key determinants of vegetation productivity in nature and as represented in terrestrial biosphere models seeking to understand land-surface atmosphere flux dynamics and its response to climate change. Non-structural carbohydrates (NSCs) and their seasonal variability are known to play a crucial role in seasonal variation of leaf phenology and growth and functioning of plants. The carbon stored in NSC pools provides a buffer during times when supply and demand of carbon are asynchronous. An example of this role is illustrated when NSCs from previous years are used to initiate leaf onset at the arrival of favourable weather conditions. In this study, we incorporate NSC pools and associated parameterizations of new processes in the modelling framework of the Canadian Land Surface Scheme-Canadian Terrestrial Ecosystem Model (CLASS-CTEM) with an aim to improve the seasonality of simulated LAI. The performance of these new parameterizations is evaluated by comparing simulated LAI and atmosphere-land CO_2 fluxes, to their observation-based estimates, at three sites characterized by broadleaf cold deciduous trees selected from the Fluxnet database. Results show an improvement in leaf onset and offset times with about 2 weeks shift towards earlier times during the year in better agreement with observations. These improvements in simulated LAI help to improve the simulated seasonal cycle of gross primary productivity (GPP) and as a result simulated net ecosystem productivity (NEP) as well.

Biogeosciences Discuss., https://doi.org/10.5194/bg-2018-168
Manuscript under review for journal Biogeosciences
Discussion started: 14 May 2018

1 Introduction

Biosphere-atmosphere interactions constitute a complex system which plays an important role in the regulation of the climate. These interactions are important determinants governing the physical and chemical properties of the atmosphere as well as the growth of plants, and result in the biosphere and atmosphere behaving as a coupled system (Pilegaard et al., 2003). Understanding this coupled behavior is a key research priority due, not only to the important role that terrestrial ecosystems play in modulating the global carbon cycle, but also to the significance of land surface characteristics for local and regional climate through biogeophysical effects (Cox et al., 2000; Prentice et al., 2001; Bonan, 2008; Franklin et al., 2016). This growing recognition of the role of land surface vegetation, and its bi-directional interactions with the climate system, has led to ever increasing complexity of the physical and biogeochemical processes that are incorporated in the land surface components of regional and global climate models (Foley et al., 1996; Sitch et al., 2008; Flato et al., 2013). Process-based land surface schemes and ecophysiological models (e.g., Running et al., 1999; Mäkelä et al., 2000; Friend et al., 2007; IPCC, 2013; Sato et al., 2015) simulate atmosphere-land exchanges of carbon, water, and energy, and offer tools for understanding vegetation behaviour for the present climate, and for projecting vegetation behaviour for future climate scenarios.

The plant canopy is a locus of physical and biogeochemical processes in an ecosystem. The functional and structural attributes of plant canopies are affected by microclimatic conditions, nutrient dynamics, herbivore activities, and many other factors (Asner et al., 2003). Leaves are the point of contact between plants and atmospheric CO_2; an increase in leaf area potentially enhances the opportunity for carbon uptake, albeit at the cost of a greater demand for water (Norby et al., 2003). The amount of foliage contained in plant canopies is one of the most basic ecological characteristics that integrates the effects of overall environmental conditions. Canopy leaf area serves as the dominant physical control over primary production (photosynthesis), transpiration, energy exchange, and other

48 physiological attributes pertinent to a range of ecosystem processes, and is therefore a core element of
49 ecological field and modeling studies (e.g., Knyazikhin et al., 1998; Xavier and Vettorazzi, 2004;
50 Aboelghar et al., 2010; Gonsamo and Chen, 2014; Bao et al., 2014; Savoy and Mackay, 2015).

51 LAI (defined as the amount of leaf area (m^2) in the canopy per unit ground area (m^2)) is a
52 dimensionless quantity and therefore can be assessed across a range of spatial scales, from individual
53 plant, a forest stand or grassland, to large regions and continents. Leaf phenology describes the
54 response of leaves to seasonal and climatic changes including the timing of bud burst, senescence (leaf
55 maturity or browning), and leaf abscission (leaf fall), and has been documented in a wide range of
56 literature (e.g., Kikuzawa, 1995; Myneni et al., 1997; Arora and Boer, 2005; Menzel et al., 2006;
57 Parmesan, 2006; Richardson et al., 2010; Dragoni et al., 2011; Smith and Hall, 2016). Leaf phenology
58 is a function of environmental conditions (in particular, temperature, soil moisture and day length). The
59 structural and adaptive qualities specific to vegetation type also determine the timing of leaf
60 phenological events. Accurate prediction of recurring vegetation cycles as a function of climate is an
61 important feature that vegetation models are expected to reproduce. The timing of bud burst and leaf
62 senescence determine the length of the growing season, and this affects gross and net primary
63 productivities (GPP and NPP), the annual cycle of LAI, and consequently, the energy, water, and
64 carbon fluxes. The seasonal progression of LAI also influences canopy conductance (Blanken and
65 Black, 2004), albedo (Sakai et al., 1997) and through its modulation of sensible and latent heat fluxes
66 (Moore et al., 1996) it also affects surface air temperatures (Levis and Bonan, 2004).

67 Despite its importance, the representation of LAI in terrestrial biosphere models is considered poor
68 (Richardson et al., 2012). Lack of high quality long term observations, the use of prescribed LAI,
69 simplified formulations of underlying biogeochemical processes, and coarse spatial resolution have
70 been mentioned as some of the limitations to accurate representation of LAI (Kucharik et al., 2006).
71 Since canopy seasonality is an important determinant of carbon (C) fluxes, poor representation of the

seasonal dynamics of LAI can lead to inaccurate estimation of vegetation productivity and consequently the net atmosphere-land CO_2 flux (Ryu et al., 2008).

Non-structural carbohydrates (NSCs) are the primary products of photosynthesis and a key energy source for plant growth and metabolism. NSCs play a central role in a plant's life processes and its response to the environmental conditions (Kozlowski, 1992; Ögren, 2000; Chatterton et al., 2006; O`Brien et al., 2014; Hartmann and Trumbore, 2016; Sperling et al., 2017). Previous studies have suggested that NSCs are stored in all plant organs (i.e., leaf, branch, root and stem) at different concentrations that vary seasonally and also inter-annualy in response to changes in environmental conditions (e.g., Oberhuber et al., 2011; Bazot et al., 2013; Mei et al., 2015). The amount of NSCs and their particular allocation to leaves, stems, and roots are considered eco-physiological traits and are among the range of adaptive strategies that plants use (Li et al., 2001; Poorter and Kitajima, 2007; Wyka et al., 2016). Many factors influence leaf NSC content, including nutrient elements (Zotz and Richter, 2006), temperature (Gough et al., 2010), precipitation (Würth et al., 2005), drought (Rosas et al., 2013), and phenology (Chen et al., 2017). Despite extensive research on the seasonal dynamics of NSC concentrations, the size and relative contributions of NSC pools across different tree organs are not well understood (Mei et al., 2015).

Plant NSC stores can compensate for a carbon or nitrogen shortage when current demand surpasses supply due to the seasonality of plant growth, stresses, or disturbances. The seasonal dynamics of NSC concentrations have been studied in various plant species (e.g., Zhu et al., 2012; Richardson et al., 2013; Saffell et al., 2014). In deciduous plants, when photosynthesis is constrained by limited leaf area and low temperature in early spring, NSC is mobilized from stem and roots to support respiration and tissue growth, resulting in decreased concentrations of NSC in these storage organs (Hoch et al., 2003; Palacio et al., 2007). During the growing season, storage pools are replenished and NSC concentration increases (Teixeira et al. 2007; Klein et al., 2016). Typically, NSC concentrations in storage organs of

Biogeosciences Discuss., https://doi.org/10.5194/bg-2018-168
Manuscript under review for journal Biogeosciences
Discussion started: 14 May 2018

the short-lived fast-growing species decrease in springtime after bud flush and then increase during the remainder of the growing season. Correspondingly, the storage organs shift from being a NSC source in the early growing season to becoming a sink in the late growing season, maintaining tree survival after the termination of photosyntate flow from aboveground sources to supply energy for stem and root tissues through the winter (Würth et al., 2005; Gough et al., 2010). During periods of limited photosynthesis, such as winter dormancy or drought stress, trees depend solely on stored NSCs to maintain basic metabolic functions, produce defensive compounds, and retain cell turgor (Sperling et al., 2015). For deciduous species, the NSC storage provides the means to jump start leaf onset by using a part of NSC stores to push leaves out at the onset of favourable weather conditions (e.g. in spring in the northern hemisphere). Representation of NSC pools is therefore an essential step for terrestrial biosphere models to better simulate leaf phenology and seasonal variability of LAI.

Here, we include a representation of NSC pools and the associated parameterizations in the framework of the Canadian Land Surface Scheme-Canadian Terrestrial Ecosystem Model (CLASS-CTEM). CLASS-CTEM exhibits delayed leaf phenology and we attempt to address this issue. In the original model, the simulated global LAI reaches its maximum in August whereas the observed LAI peaks in July (e.g., see Fig. 11 of Anav et al., 2013). The objective of this study is to improve and assess the performance of CLASS-CTEM simulated leaf phenology for broadleaf cold deciduous trees. Model performance is evaluated against in situ measurements from three sites from the Fluxnet data network (*https://fluxnet.ornl.gov/obtain-data*) which provides tower-based meteorological variables used to drive the model as well as observations of LAI, carbon, and energy fluxes.

2 Model, data, and methods

Biogeosciences Discuss., https://doi.org/10.5194/bg-2018-168
Manuscript under review for journal Biogeosciences
Discussion started: 14 May 2018

119 **2.1 CLASS-CTEM model**

120 A coupled version of the Canadian Land Surface Scheme (v. 3.6; Verseghy, 2012) and Canadian
121 Terrestrial Ecosystem Model (v. 2.1.1, Melton and Arora 2014) (CLASS-CTEM) is used here. Slightly
122 older versions of both models are currently implemented in the second generation Canadian Earth
123 System Model (CanESM2; Arora et al., 2011). While CLASS simulates fluxes of energy, water, and
124 momentum at the land-atmosphere boundary, atmosphere-land fluxes of CO_2 are simulated by CTEM.
125 CLASS operates at a typical time step of 30 minutes and prognostically simulates the liquid and frozen
126 soil moisture and soil temperature for its multiple soil layers (3 layers are employed here with
127 maximum thicknesses of 0.1, 0.25 and 3.75 m); the temperature, thickness and fractional cover of
128 snow; and the temperature and amount of snow and rain on the vegetation canopy. The permeable
129 depth of the soil column may be smaller than the total depth of the soil layers employed; if a layer
130 spans the permeable depth boundary it is subdivided for hydrological calculations. CLASS
131 distinguishes four plant functional types (PFTs) (needleleaf trees, broadleaf trees, crops, and grasses) as
132 shown in Table 1. CLASS calculates net radiation (R_n) based on prognostically calculated land surface
133 albedo and the skin temperature of the land surface (T_s) as

134 $$R_n = SW(1-\alpha) + LW - \sigma {T_s}^4 \quad (1)$$

135 where α is albedo, SW and LW are incoming short and long wave radiation, σ is the Stefan-Boltzman
136 constant. R_n is partitioned into latent (LE), sensible (H), ground, and canopy heat fluxes. When in
137 equilibrium and over annual and longer time periods, since ground or canopy do not gain or lose heat
138 systematically, the sum of latent and sensible heat fluxes equals net radiation (R_n = LE + H).

139 CTEM simulates terrestrial processes by prognostically tracking carbon in three living vegetation
140 components (leaves, stems and roots) and two dead carbon pools (litter and soil) for seven non-crop
141 and two crop PFTs that map directly onto CLASS' PFTs (Table 1). The terrestrial ecosystem processes

Biogeosciences Discuss., https://doi.org/10.5194/bg-2018-168
Manuscript under review for journal Biogeosciences
Discussion started: 14 May 2018

simulated in this study include photosynthesis, autotrophic respiration, heterotrophic respiration, dynamic leaf phenology, and allocation of carbon from leaves to stem and root components. These processes are described in a sequence of papers detailing parameterization of photosynthesis, autotrophic and heterotrophic respiration (Arora, 2003), dynamic root distribution (Arora and Boer, 2003), phenology, carbon allocation, biomass turnover and conversion of biomass to structural attributes (Arora and Boer, 2005). A full description of CTEM can be found in the appendix of Melton and Arora (2016).

The structure of CTEM is shown in Fig. 1; the original three live vegetation pools (leaves, stem, and roots) are indicated by L, S, and R subscripts, respectively), and the two dead carbon pools (litter or detritus and soil carbon) are indicated by D and H subscripts, respectively). Time varying fluxes in and out of these carbon pools (C_L, C_S, C_R, C_D, and C_H; in $kgCm^{-2}$) makes them prognostic variables in the model. The corresponding rate change equations for amount of carbon in the three live vegetation components (leaves, stem, and roots) in the original model version are represented by

$$\frac{dC_i}{dt} = a_{f_i}\left(G - E_m - E_g\right) - D_i = a_{f_i}N - D_i \quad (2)$$

where the index *i* corresponds to each of the live vegetation pools ($i = L, S, R$), a_{f_i} represents allocation fraction for a given vegetation component, G is canopy gross primary productivity, E_m is vegetation maintenance respiration, E_g is vegetation growth respiration, D_i represents the litter loss. $N = G - E_m - E_g$ is the canopy net primary productivity (NPP) and therefore $a_{f_i}N$ represents fraction of NPP allocated to the three vegetation components. Growth respiration, E_g, is estimated as a fraction of the positive gross canopy photosynthetic rate after maintenance respiration has been accounted for (equation A28, Melton and Arora (2016)). $E_a = E_m + E_g$ is the autotrophic respiration, therefore, $N = G - E_a$. When heterotrophic respiration (E_h) is accounted for, net ecosystem productivity (NEP) is calculated as $NEP = G - E_a - E_h = N - E_h$. Positive NEP values indicate that land is gaining carbon

Biogeosciences Discuss., https://doi.org/10.5194/bg-2018-168
Manuscript under review for journal Biogeosciences
Discussion started: 14 May 2018

165 from the atmosphere. Combined autotrophic and heterotrophic respiration (E_a + E_h) are referred to as
166 the ecosystem respiration (E_r).
167
168 **2.1.1 Addition of NSC pools**
169 For the modifications made in this study, first, NSC pools are included in each of the live
170 vegetation components (leaves, stem, and roots). The total biomass (Kg C m^{-2}) for each of these
171 components is divided into its non-structural and structural components (indicated by subscripts NS
172 and S) as shown in Figure 1. $C_L = C_{L,NS} + C_{L,S}$ and similarly for C_S and C_R. The fraction of NPP
173 allocated to each live vegetation component is first moved to its non-structural part, and a flux of
174 carbon from the non-structural to the structural part provides carbon to the structural part. Once the
175 carbon is moved from non-structural to a structural part of a component it cannot be moved back. Since
176 NPP includes respiratory losses, this essentially implies that respiratory carbon losses are assumed to
177 occur from the non-structural part. Litter losses, on the other hand, occur from both the structural and
178 non-structural parts of leaves, stem and root components.
179 The modified rate change equations for carbon in the non-structural and structural parts of leaf (Eq.
180 3) and stem and root (Eq. 4) components are thus written as
181

182 $$\begin{aligned} \frac{dC_{L,NS}}{dt} &= a_{f_L}N - D_{L,NS} - F_{ns2s,L} + T_S + T_R \\ \frac{dC_{L,S}}{dt} &= F_{ns2s,L} - D_{L,S} \end{aligned} \quad (3)$$

183 $$\begin{aligned} \frac{dC_{j,NS}}{dt} &= a_{f_i}N - D_{j,NS} - F_{ns2s,j} - T_j \\ \frac{dC_{j,S}}{dt} &= F_{ns2s,j} - D_{j,S} \end{aligned} \; ; j = S, R \quad (4)$$

184

Biogeosciences Discuss., https://doi.org/10.5194/bg-2018-168
Manuscript under review for journal Biogeosciences
Discussion started: 14 May 2018

where $F_{ns2s,i}(i = L, S, R)$ represents carbon flux from the non-structural to structural part of a component (leaf, stem or root), and $T_j(j = S, R)$ represents the reallocation (or transfer) of carbon from stem and root components to leaves during leaf out period. Note that there are no autotrophic respiration terms in equations (3) and (4) since they are already included in the term *N*, the net primary productivity. $F_{ns2s,i}$ is represented as

$$F_{ns2s,i} = \mu_i a_{f_i} Nmax\left[0, \left(\eta - \eta_{i,min}\right)\right] \quad (5)$$

where μ_i is a non-dimensional coefficient set to 70. Equation (5) attempts to keep the fraction of non-structural to total carbon in a component $\eta_i = C_{i,NS}/C_i$ above its minimum specified value $\eta_{i,min}$. During periods of negative NPP, for e.g. as is the case during winter for cold deciduous trees when they do not have their leaves on, $F_{ns2s,i}$ is set to zero. This represents the attempts by plants to conserve their NSC pools during a period of no productivity. The amount of carbon in non-structural and structural parts of all vegetation components are time varying variables and therefore so is the ratio of non-structural to total carbon (η_i). The minimum ratio of non-structural to total carbon in a component $(\eta_{i,min})$ is specified to be 0.05 for the broadleaf cold deciduous PFT considered here, following Li et al. (2016).

The above modifications made to version 2.1.1 of CTEM in regards to the inclusion of NSC pools allow the movement of non-structural carbohydrates between the model's three live vegetation components, in particular, reallocation of non-structural carbohydrates from stem and root components for leaf out at the onset of spring for the broadleaf cold deciduous tree PFT. In addition, we also adjust allocation fractions for the leaves, stem and root components after summer solstice in response to day length, and the lower temperature thresholds for leaf litter generation due to cold stress. Deciduousness at high latitudes is determined both by day length and temperature (Xie et al., 2015) and these modifications, discussed below, help to improve simulated leaf phenology.

Biogeosciences Discuss., https://doi.org/10.5194/bg-2018-168
Manuscript under review for journal Biogeosciences
Discussion started: 14 May 2018

208

209 **2.1.2 Reallocation of non-structural carbon during leaf out period**

210 Leaf phenology in CTEM is represented via four phenological states a plant can be in at any given
211 time (Arora and Boer, 2005). These stages include no leaves or dormant state, maximum leaf growth
212 state, normal growth state, and leaf fall or harvest state. Depending on their deciduousness, CTEM's
213 nine plant functional types (Table 1) may or may not go through these four different leaf phenological
214 states. A broadleaf cold deciduous tree, transitions through all four states in a year: leafless/dormant
215 state in winter, maximum growth state (following arrival of favorable climatic condition in spring when
216 all NPP is allocated to leaves), normal growth state (after reaching a threshold LAI, NPP is allocated to
217 stem and roots in addition to leaves), and finally the leaf fall state (triggered by unfavorable
218 environmental conditions and with no carbon allocation to leaves). When all the leaves have been shed,
219 the trees go back into the leafless or dormant state again and the cycle repeats itself in the next year.

220 In the original version of the model, when a plant moves into the maximum leaf growth state all
221 NPP is allocated to leaves until a threshold LAI (L_{thrs}, m^2/m^2) has been grown. L_{thrs} is about 40%-
222 50% of the maximum LAI a plant can support depending on its stem and root biomass and based on an
223 allometric relationship between green and woody biomass (Melton and Arora, 2016). In the absence of
224 NSC pools in the original model version, photosynthesis during the early leaf out period is based on a
225 small imaginary amount of leaves (referred to as storage LAI). Once the actual LAI exceeds the storage
226 LAI then photosynthesis is based on the actual LAI. Storage LAI is proportional to a plant's stem and
227 root biomass and was intended as a proxy for the size of NSC pools. However, the rate of
228 photosynthesis from a reasonably apportioned storage LAI is still too small to realistically 'push out'
229 leaves at the onset of spring in a time period of about two weeks as seen in observations. This
230 limitation in the original model version is overcome here with the inclusion of NSC pools. In the
231 modified version of the model used here, a specified fraction of carbon amount needed to reach the

Biogeosciences Discuss., https://doi.org/10.5194/bg-2018-168
Manuscript under review for journal Biogeosciences
Discussion started: 14 May 2018

threshold LAI is reallocated ($T_j, j = S, R$) from a plant's stem and root NSC pools to the non-structural part of leaves every day until LAI reaches L_{thrs}. Note that while this reallocation occurs the leaves are still able to photosynthesize and able to increase their biomass as in the original model version, depending on meteorological conditions. The objective of carbon reallocation from stem and roots to leaves is to accelerate the rate of leaf expansion and LAI increase during leaf onset.

The amount of carbon reallocated (kg C/m^2) from stem and root components to leaves is given by

$$T_j = \beta \frac{L_{thrs}}{SLA} f_j; j = S, R \quad (6)$$

$$f_j = \begin{Bmatrix} \frac{C_{j,NS}}{C_{S,NS}+C_{R,NS}} & if \eta_j > \eta_{j,min} \\ 0 & if \eta_j \leq \eta_{j,min} \end{Bmatrix}; j = S, R \quad (7)$$

where SLA is the specific leaf area (m^2/kg C), β is the reallocation coefficient set to 6.66x10^{-3} and fractions $f_j (j = S, R)$ ensure that carbon reallocated from stem and root NSC pools is proportional to the size of their NSC pools. Equation (7) also shows that when the fraction of NSC pool relative to total carbon in a component $(\eta_j = C_{j,NS}/C_j), j = S, R$ is equal to or drops below its minimum specific value $(\eta_{j,min})$ then reallocation is stopped. Reallocation is only performed during the leaf out state when trees are in the maximum leaf growth state.

2.1.3 Adjustments to allocation fraction to leaves after the summer solstice

CTEM uses dynamically calculated allocation fractions (Arora and Boer, 2005; Melton and Arora, 2016) for leaves, stem, and roots, which are based on the light, water, and leaf phenological status of vegetation. The allocation to the three live vegetation components is based on assumptions that carbon is preferentially allocated: 1) to roots when soil moisture is limiting, 2) to leaves when LAI is low, and 3) to stem to increase vegetation height and lateral spread when increasing LAI leads to a decrease in

Biogeosciences Discuss., https://doi.org/10.5194/bg-2018-168
Manuscript under review for journal Biogeosciences
Discussion started: 14 May 2018

254 light penetration. These allocation fractions are superseded by three additional rules: 1) all carbon is
255 allocated to leaves at the time of leaf out for cold deciduous tree PFTs to accelerate leaf development,
256 2) allocation fractions are adjusted when necessary to ensure a tree has enough stem and root biomass
257 to support leaves (to satisfy a structural allometric relationship), and 3) a minimum realistic root to
258 shoot ratio is maintained for all PFTs.

259 When compared to observation-based estimates of globally-averaged LAI, CLASS-CTEM
260 simulated LAI shows a much slower rate of decline after reaching its annual maximum, which typically
261 occurs just after the summer solstice in each hemisphere (Anav et al., 2013). To address this issue
262 allocation to leaves of cold deciduous tree PFTs after summer solstice is reduced by multiplication with
263 a day-length dependent factor (Γ) given by

264 $$\Gamma = \left[\frac{d}{d+(d_{max}-d)0.5\left(tanh\left(\frac{\pi}{180}(20\phi-800)\right)+1\right)}\right]^{20} \quad (8)$$

265 $$d = 24 - \frac{24}{\pi} acos\left[max\left(-1, min\left(\frac{sin\phi sin\delta_c}{cos\phi cos\delta_c}, 1\right)\right)\right] \quad (9)$$

266

267 where d is the day length at latitude ϕ (radian), d_{max} is its maximum value (hour), and δ_c (radians) is
268 solar declination. Γ varies between 0 and 1 and its behaviour in Figure 2 shows how allocation to
269 leaves is reduced at a faster (slower) rate closer to poles (equator) after summer solstice in the northern
270 hemisphere (June 21). Below 30°N in the northern hemisphere equation (8) yields $\Gamma = 1$ so allocation
271 fraction for leaves is not modified. Deciduousness due to day length and temperature typically does not
272 occur in tropics where it is primarily controlled by soil moisture. Neither do broadleaf deciduous cold
273 trees typically exist in the tropics. Similar behaviour is obtained for the southern hemisphere after
274 December 21. Since the allocation fractions for leaves, stem, and root components should add to 1 the

Biogeosciences Discuss., https://doi.org/10.5194/bg-2018-168
Manuscript under review for journal Biogeosciences
Discussion started: 14 May 2018

decrease in allocation fraction for leaves implies an increase in allocation fraction for stem and root components in the modified version of the model.

2.1.4 Adjustments to the lower air temperature threshold

The CLASS-CTEM model is able to respond to environmental conditions and to transition between different leaf phenological states (Arora and Boer, 2005). Leaf litter (D_L) generation is caused by normal turnover of leaves as well as drought and cold stresses which all contribute to LAI seasonality.

$$D_L = C_L\left[1 - e^{(-\Omega_N - \Omega_C - \Omega_D)}\right] \quad (10)$$

where C_L is the leaf carbon pool and $\Omega_{N,C,D}$ are the leaf loss rates (day^{-1}) associated with normal turnover of leaves and the cold and drought stresses. The leaf loss rate associated with cold stress (Ω_C) is based on Eqs. A49-50 of Melton and Arora (2016) (shown below as Eq. 11)

$$\Omega_C = \Omega_{C,max} L_{cold}^3 \quad (11)$$

where $\Omega_{C,max}$ is the maximum leaf loss rate due to cold stress and L_{cold} is a scalar that varies between 0 and 1 as follows

$$L_{cold} = \begin{cases} 1 & , T_a < \left(T_{cold}^{leaf} - 5\right) \\ 1 - \frac{T_a - \left(T_{cold}^{leaf} - 5\right)}{5} & , \left(T_{cold}^{leaf} - 5\right) < T_a < T_{cold}^{leaf} \\ 0 & , T_{cold}^{leaf} < T_a \end{cases} \quad (12)$$

T_{cold}^{leaf} is a PFT dependent parameter below which a PFT experiences damage to its leaves and this promotes leaf loss due to cold stress in the model.

The original version of the model used a T_{cold}^{leaf} parameter value of 8 °C throughout the year. In the modified version of the model used here for the broadleaf cold deciduous tree PFT a T_{cold}^{leaf} value of 12 °C is used after summer solstice. For broadleaf cold deciduous tree PFT, leaf out starts in spring, the maximum LAI occurs between July to September (during the northern hemisphere's summer) and the

Biogeosciences Discuss., https://doi.org/10.5194/bg-2018-168
Manuscript under review for journal Biogeosciences
Discussion started: 14 May 2018

296 leaves are shed between October and November during autumn. Increasing T_{cold}^{leaf} leads to more leaf
297 litter generation due to the cold stress in the autumn and moves the descending side of the LAI curve
298 inwards during autumn.
299
300 **2.2 Model evaluation and experimental set up**
301
302 **2.2.1 Description of Fluxnet sites**
303 We evaluate the performance of the original and modified versions of the CLASS-CTEM
304 framework in simulating leaf phenology at three well studied sites in the Eastern United States (Fig. 3)
305 which are selected from the Fluxnet network: (1) Harvard Forest (US-Ha1) located at 42.53 ºN and
306 72.17 ºW, (2) Morgan Monroe State Forest (US-MMS) at 39.32 ºN and 86.41 ºW, and (3) University of
307 Michigan Biological Station (US-UMB) at 45.55 ºN and 84.71 ºW. The location of the three Fluxnet
308 sites is shown in Figure 3. The selected sites meet our requirement of availability of observation-based
309 LAI data (against which our model results can be evaluated) and are primarily characterized by
310 deciduous broadleaf forests although with different species composition. The mean annual climate at
311 these sites and their species composition are summarized in Table 2. While these sites differ somewhat
312 in the climate they experience, they share enough commonalities in climate to exhibit similar seasonal
313 dynamics of LAI. Annual precipitation at these temperate locations (US-Ha1, US-MMS, and US-
314 UMB) is 1189, 1083, and 613 mm, with an annual mean temperature of 8.2, 12.4, and 7.2 ºC for each
315 site, respectively. These annual averages are based on the half-hourly meteorological data that are used
316 to drive the CLASS-CTEM model for the time period summarized in Table 2.
317 The US-Ha1 site is owned by Harvard University. Most of its surrounding area was cleared for
318 agriculture during European settlement in 1600-1700. The trees at the site have been regrowing since

before 1900 and are currently characterized by predominantly red oak and red maple, with patches of mature hemlock stand and individual white pine. Climate measurements have been made at the Harvard Forest since 1964. The US-MMS site is owned by the Indiana Department of Natural Resources. Many of trees in the tower footprint are 60-80 years old. Today, the forest is a secondary successional broadleaf forest within the maple-beech to oak-hickory transition zone of the eastern deciduous forest. Finally, the US-UMB site is located within a protected forest owned by the University of Michigan and consists of mid-aged northern hardwoods, conifer understory, aspen, and old growth hemlock.

The permeable soil depths are specified at 2.5, 2.5, 2.62 m at the US-Ha1, US-MMS, and US-UMB sites, respectively. Soil texture information was adapted from the global data set of Zobler (1986) and used to specify the percentage of sand and clay in the model's three soil layers as follows. At US-Ha1, the percentages of sand in the first, second and third soil layers are specified at 68.5, 66.5, and 72.25%, and the percentage of clay at 5, 5 and 4.25%, respectively. At US-MMS, the percentages of sand in the first, second and third soil layers are specified at 21, 22.5 and 30.25%, and the percentage of clay at 21, 23 and 23.75%, respectively. At US-UMB, the percentages of sand in the first, second and third soil layers are specified at 71, 72.5 and 73.25%, and the percentage of clay at 7, 7 and 7.75%, respectively.

2.2.2 CLASS-CTEM simulations

For the three sites investigated here, we have used version 3.6 of the CLASS coupled to version 2.1.1 of the CTEM model and made changes mentioned above in Section 2.1. Model performance is evaluated for both the modified and original (without NSC pools) versions against available observation-based estimates of LAI, and energy and CO_2 fluxes. Simulations were performed for the broadleaf cold deciduous tree PFT with 100% fractional cover.

Biogeosciences Discuss., https://doi.org/10.5194/bg-2018-168
Manuscript under review for journal Biogeosciences
Discussion started: 14 May 2018

342 Seven meteorological variables are required to drive the CLASS-CTEM model - air temperature,
343 air pressure, wind speed, incoming short wave radiation, incoming long wave radiation, precipitation,
344 and specific humidity. Gap-filled meteorological forcing was obtained for each of the three Fluxnet
345 sites. The data were either available at a half-hourly time step or were linearly interpolated from hourly
346 to half-hourly resolution. A specified CO_2 concentration of 350 ppm was used at all sites. The
347 meteorological data used to drive the model correspond to the period 1998-2013 for the site in Harvard
348 forest, 1999-2006 for the site in Morgan Monroe State Forest and 1997-2013 for the site at the
349 University of Michigan Biological Station.

350 All simulations were forced with meteorological data from their respective Fluxnet sites repeatedly
351 until model carbon pools reached equilibrium and the annually averaged NEP was close to zero.
352 Although not perfect, in the absence of full histories of disturbance and meteorological data at these
353 sites this approach still allows comparison of the seasonality of simulated LAI and primary carbon and
354 energy fluxes with observation-based estimates once the model pools reach equilibrium. The
355 disturbance (fire) module was not activated in these simulations. Observation-based LAI measurements
356 were obtained from the Ameriflux web site (*https://ameriflux.lbl.gov*). Energy and CO_2 fluxes were
357 obtained from the Fluxnet web site (*https://fluxnet.fluxdata.org*).

358

359 **3 Results**

360 Model performance is evaluated by comparing simulated LAI and CO_2 fluxes of gross primary
361 productivity (GPP) and net ecosystem productivity (NEP) which is our primary focus. We also
362 compare radiative energy fluxes of net radiation and latent and sensible heat with their observation-
363 based estimates from the modified and the original model versions.

364

365 **3.1 LAI and land-atmosphere CO_2 fluxes**

Biogeosciences Discuss., https://doi.org/10.5194/bg-2018-168
Manuscript under review for journal Biogeosciences
Discussion started: 14 May 2018

366 Figures 4-6 compare simulated values of LAI, GPP, NEP, and E_r from the two model versions with
367 their observation-based estimates at the US-Ha1, US-MMS, and US-UMB Fluxnet sites. Observation-
368 based measurements are shown in black and simulated mean daily values are shown in red (for the
369 original model version indicated as CLASS-CTEM Original) and blue (for the modified version, with
370 NSC pools and other changes indicated as CLASS-CTEM Modified). Just like simulated values, the
371 observation-based estimates also represent average daily values across all years for which the data were
372 available. The figure legends, in addition to identifying the two model versions and observations, also
373 show the mean annual value of the quantity plotted. The mean annual values of LAI, GPP, E_r, and NEP
374 are also summarized in Table 3. At all sites, when compared to the original version, the modified
375 version of the model shows a phenological shift of about 2 weeks earlier in the year which is in better
376 agreement with observed LAI transitions (Figs. 4-6, panel a). The timing of maximum LAI also
377 improves and shows a shift of about 2 months earlier in the year, from late September and early
378 October to late July and early August. The observation-based estimates of LAI suggest the presence of
379 understory vegetation at two of the three Fluxnet sites (the Monroe and the Michigan sites). The
380 CLASS-CTEM modelling framework does not represent any understory vegetation. Despite this, the
381 model still overestimates maximum LAI at all locations and its implications are discussed below. At all
382 three sites, the inclusion of non-structural carbon pools (section 2.1.1) and other model modifications
383 (sections 2.1.2 to 2.1.4) produces a notable improvement in simulated LAI seasonality, especially
384 during canopy development (i.e., spring and early summer) and its autumn decline.

385 The Morgan Monroe site (Fig. 5) experiences somewhat warmer temperatures than the Harvard and
386 Michigan sites (Figs. 4 and 6) (mean annual temperature at the Morgan Monroe is about 4 ºC higher
387 than at the other two sites, see Table 2) and as a result the growing season is somewhat longer at the
388 Morgan Monroe site. The model is able to successfully capture this difference amongst the sites.
389 Overall, the simulated GPP and NEP (Figs. 4-6, panels b and c) compare reasonably well with

observations. Improvements in simulated LAI seasonality lead to concomitant improvements in simulated GPP especially at the ascending side of the plots when the growing season starts. In the original version of the model the increase in GPP at the start of the growing season is delayed due to delayed leaf out. Note that the simulated GPP values compare well with their observation-based estimates despite the higher simulated LAI. Improvements in simulated GPP also lead to improvements in simulated NEP in Figures 4-6 (panel c), and similar to GPP, especially on the ascending side of the plots at the start of the growing season. The annual mean of observation-based NEP values (as shown in the figure legends) is positive because northern hemisphere temperate land is currently a sink of carbon (Myneni et al., 2001). In contrast, the annual mean of simulated NEP values is close to zero by construction, because the model was spun-up to an equilibrium state. The positive annual mean of observation-based NEP values, compared to simulated NEP values, can manifest in multiple ways – as primarily higher summer values when NEP values are positive (as for the Harvard forest site), as higher values through the year (as is mostly the case at the Morgan Monroe site) and as less negative NEP values during non-growing season when NEP values are negative (as seen at the University of Michigan site). Regardless of this caveat, the inclusion of NSC pools to advance leaf onset and offset times does lead to an improvement in seasonality of simulated NEP values.

While photosynthesis primarily depends on the current meteorological conditions and LAI amongst other environmental factors (including atmospheric CO_2 concentration), ecosystem respiration (Figs. 4-6, panel d) depends strongly on the vegetation and soil carbon pool sizes. As a result, if simulated vegetation and soil carbon pools are larger or smaller than observation-based estimates then so would be the respiratory fluxes. The model is spun up to equilibrium at specified atmospheric CO_2 concentration of 350 ppm while the real world forests have experienced a gradual increase in atmospheric CO_2 concentration, changes in climate, and disturbances over their life time. Thus modelled vegetation and soil carbon pools cannot be expected to be exactly the same as in the real

Biogeosciences Discuss., https://doi.org/10.5194/bg-2018-168
Manuscript under review for journal Biogeosciences
Discussion started: 14 May 2018

414 world but still expected to be reasonable. Note also that the simulated annual respiratory fluxes are
415 higher than observed at all three sites (Figs. 4-6, panel d, and Table 3). Had the simulated fluxes been
416 lower than what they are now and closer to their observation-based estimates, then the simulated NEP
417 would have been more similar to observations. We have chosen to use atmospheric CO_2 concentration
418 of 350 ppm to spin up the model pools (while the average CO_2 concentration during the first decade of
419 the 21st century was around 380 ppm) because the terrestrial biosphere is currently not in equilibrium
420 with the atmospheric CO_2 concentration. Nevertheless, the model simulates the seasonality of
421 ecosystem respiratory fluxes reasonably well. In absence of the long term disturbance history or
422 meteorological data to drive the model with, the current methodology (where the model is driven
423 repeatedly with the available observed meteorological data) is reasonable and allows us to assess the
424 seasonality of simulated LAI and land-atmosphere CO_2 fluxes - which is the primary objective of our
425 study.
426
427 **3.2 NSC pools**
428 Figures 7-9 evaluate the seasonal cycle of the NSC pools in leaf, stem, and root vegetation
429 components at US-Ha1, US-MMS, and US-UMB Fluxnet sites, respectively. There are no observation-
430 based estimates of NSC pools available at the three Fluxnet sites. For the broadleaf cold deciduous tree
431 PFT considered here, the stem carbon pool is the largest (and so are its structural and non-structural
432 parts) and the leaf carbon pool is the smallest (Figs. 7-9, panels a and c). The amount of non-structural
433 carbon reallocated from the stem and root NSC pools to leaves during leaf onset in early spring (see
434 section 2.1.2) is shown in Figures 7-9 (panel b). Figures 7-9 (panel d) show the seasonality of the
435 carbon flux from the non-structural to the structural part of the leaf, stem and root components for the
436 three sites. The seasonality of total stem and root carbon pools is driven mostly by the seasonality of
437 their non-structural parts.

Biogeosciences Discuss., https://doi.org/10.5194/bg-2018-168
Manuscript under review for journal Biogeosciences
Discussion started: 14 May 2018

For the stem and root components, the non-structural parts contribute about 6-10% to the total pool size. During the early leaf-out period when reallocation from stem and root NSC pools to leaves is taking place (section 2.1.2), the stem's NSC pool gets depleted. This transfer/reallocation stops after a threshold LAI is achieved. The transfer of NSC from stem and root pools to leaves occurs mostly through the stem (see Figs. 7-9, panel b) since its NSC pool is about 3-4 times larger than the root component. The NSC pool for both components reduces during the period when leaves are not present (and GPP is zero) due to respiratory and litter losses. The pools for both stem and root components get replenished later during the growing season when a sufficient amount of leaves has been grown and allocation of carbon to stem and root components is restored. This is seen in Figures 7-9 (panel d) which show the flux of carbon from non-structural to structural leaf, stem and root components. Early on during the growing season, carbon flux from the leaf NSC pool to its structural part is much higher since the model preferably allocates carbon to leaves as discussed in section 2.1.2. After a threshold LAI is reached, carbon is also allocated to stem and root NSC pools which subsequently start to allocate carbon to their structural pools and the tree biomass continues to increase. At the end of the growing season, when photosynthesis stops, allocation to all three components and the fluxes from NSC to structural parts terminate. During the dormant winter season NSC pools provide for the respiratory costs.

3.3 Energy fluxes

Figure 10 compares observation-based measurements of latent heat (LE), sensible heat (H), and net radiation (R_n) fluxes at the three Fluxnet sites, with their simulated values from the two model versions. Annual mean values of these observation-based and simulated radiative and turbulent energy fluxes are also summarized in Table 3. Unlike the simulated fluxes, the annual mean sum of the observed LE and H, averaged over the years for which observations are available, is not equal to the observed R_n. This

Biogeosciences Discuss., https://doi.org/10.5194/bg-2018-168
Manuscript under review for journal Biogeosciences
Discussion started: 14 May 2018

462 non-closure of the energy budget is seen at all three sites and is a typical characteristic of eddy
463 covariance based flux measurements (Gao et al., 2017). The annual energy budget closure is off by
464 17% at the University of Michigan Biological Station , 20% at the Harvard Forest and 30% at the
465 Morgan Monroe sites as seen in Table 3. Keeping this caveat in mind, the model overall captures the
466 seasonality of radiative and turbulent fluxes shown in Fig. 10 reasonably, with the exception of late
467 winter and early spring. During this period, as solar radiation increases R_n is underestimated (Fig. 10,
468 panels a-c) until the canopy approaches a full-leaf state and this leads to an underestimation of H (Fig.
469 10, panels g-i) and overestimation of LE. This may be caused by an overestimation of canopy
470 transmissivity and underestimation of snow and soil masking by leafless forests with increasing solar
471 elevation (recently observed in unpublished simulations with CLASS-CTEM at the Borden forest,
472 Borden, Ontario), and may also be exacerbated by the lack of representation of a small evergreen
473 needleleaf fraction at US-Hal and a conifer understory at US-UMB. LE is apparently overestimated
474 throughout the year at US-MMS but we suspect this reflects a larger underestimation of LE relative to
475 H in the measured fluxes; Oliphant et al. (2004) found that accounting for long sampling tube damping
476 effects on LE resulted in a 16% improvement in energy balance closure at this site. The change to an
477 earlier leaf phenology in the modified simulations results in a slightly earlier increase in LE in the
478 spring, as well as slightly earlier decreases in autumn at US-Hal and US-UMB, but differences are
479 much smaller at US-MMS.
480
481 **4. Discussion and conclusions**
482 The CLASS-CTEM model, similar to other land surface schemes implemented in other Earth
483 system models, is not tuned for any specific location but is expected to behave realistically at all
484 locations. Model processes correspond to generic PFTs, in this case broadleaf cold deciduous trees, and
485 are not meant to represent specific species differences within a PFT. It is nearly impossible, at present,

to determine the more than 100 parameters that the model uses for individual species. As a result, while our three chosen sites are characterized by different species (as shown in Table 2) they must be represented by a single set of parameter values which correspond to the broadleaf cold deciduous PFT.

Previous studies using the CLASS-CTEM model in the context of land-atmosphere CO_2 fluxes and simulated carbon pools have evaluated its performance at point (Arora, 2003; Arora and Boer, 2005; Melton et al., 2015), regional (Garnaud et al., 2015; Peng et al., 2014; Arora et al., 2016) and global (Arora and Boer, 2010; Melton and Arora, 2014, 2016) scales. These studies indicate that the model performance is reasonable. CLASS-CTEM also participated in the TRENDY model intercomparison, the result of which contributed to the Global Carbon project for years 2016 and 2017 (Le Quéré et al., 2016, 2017). A typical model evaluation exercise at the global and regional scale compares model-simulated geographical distribution of GPP, vegetation biomass, and soil carbon with their respective observation-based estimates. Point scale studies, on the other hand, typically focus on the simulated seasonality of energy and CO_2 fluxes as is the case in this study. Model evaluation exercises not only help in identifying model limitations but also yield opportunities to improve model performance by tuning model parameters.

Previous evaluations of the CLASS-CTEM model that highlighted its limitation of delayed leaf phenology (e.g., Anav et al., 2013) were the motivation for this study. NSC pools play an important role during leaf onset for broadleaf deciduous cold trees, but also other PFTs, and their effect in the original model was represented using the concept of imaginary leaves whose LAI is assumed to be directly proportional to non-leaf biomass. Here, we have included NSC pools in the model framework explicitly along with some other changes and these modifications do lead to improvement in simulated leaf phenology and concomitant improvements in simulated seasonal cycle of GPP and NEP. Improvements in simulated energy fluxes are much harder to detect because the observation-based energy fluxes are affected by non-closure of the energy budget but also because latent heat fluxes are

not as strongly dependent on LAI as GPP. Transpiration from plants and evaporation of intercepted water on canopy leaves are not the only part of the total evapotranspirative flux. Evaporation also occurs from water in the soil and through sublimation of snow.

Despite the simulated LAI being higher than observation-based estimates the simulated GPP, E_r, and NEP compare reasonably with their observation-based estimates. Possible reasons for higher simulated LAI include higher than observed allocation to leaf compared to stem and root components and lower than observed leaf turnover and/or leaf respiration rates. The model currently uses a maximum photosynthetic rate (V_{max}) value of 57 u-mol CO_2/m^2s for broadleaf cold deciduous trees based on Table 3 of Kattge et al.(2009) who derive V_{max} values for major PFTs using more than 700 data estimates. Simulated GPP in the model is directly proportional to V_{max}. While the model simulated LAI can be lowered by tuning allocation to leaves, leaf turnover and/or respiration rates specifically for these sites, this would imply using a V_{max} value higher than that suggested by Kattge et al.(2009) to achieve realistic GPP. It is possible that the average V_{max} value derived by Kattge et al.(2009) is not representative of broadleaf cold deciduous trees in the Eastern United States. The simulated LAI in the model is the result of multiple model processes interacting with each other. We note this limitation of the model at these locations and plan to address it in near future. While LAI is an important determinant of model performance even more important are the land-atmosphere CO_2 fluxes from an ESM perspective since it is the CO_2 fluxes which determine the carbon budget of the atmosphere in a fully coupled ESM simulation (Arora et al., 2013).

Plants are extremely complex living organisms which respond to the changes in their physical and chemical environmental conditions using a myriad of adaptations. Our limited understanding of these adaptations comes only from empirical observations of their behaviour and measurement of their physical and chemical responses to environmental changes. Models typically represent only a fraction of this understanding because model structures depend on the purpose of the model and the amount of

534 details that can be represented reasonably in a global application. In hindsight, the omission of NSC
535 pools in the original model version was a structural error and while the conceptual imaginary leaves
536 tried to mimic the fast growth rate of leaves during leaf onset at the arrival of favourable environmental
537 conditions they were not completely successful in capturing the real-world behaviour. Unlike physical
538 models, which describe a physical process, modelling of biological response to changes in
539 environmental conditions is more complex. While there may be underlying physical laws that
540 determine the response of plants to changes in environmental conditions, we can only interpret this
541 with a biological point of view. Dynamic vegetation models and land surface schemes parameterize
542 biological functioning using mathematical formulations to reproduce empirical observations and
543 modellers' conceptual understanding of how the biology works. The inclusion of NSC pools in the
544 CLASS-CTEM framework is based on the same philosophy.

545 The implementation of NSC pools in the CLASS-CTEM modelling framework presented in this
546 study is meant specifically to address the problem of delayed leaf phenology. NSC pools also play a
547 vital role in the overall health of the plants. During periods of limited photosynthesis, trees depend
548 solely on stored NSCs to maintain basic metabolic functions, produce defensive compounds, and retain
549 cell turgor (Sperling et al., 2015). A period of continuous drought, for instance, will gradually reduce
550 the size of NSC pools and this can be used as a trigger to initiate drought related mortality in the model,
551 or alternatively NSC pools may be used to allow leaf growth during a short-term dry period to
552 represent resilience (Mitchell et al., 2013). The inclusion of NSC pools also lays the groundwork to
553 implement a nitrogen (N) cycle in the CLASS-CTEM framework since modelling V_{max} as a function of
554 leaf N content requires leaf N content in the non-structural part of the leaves.

555 In conclusion, modifications to the CLASS-CTEM framework made in this study to address the
556 problem of delayed leaf phenology yield improvements to simulated seasonality of LAI at the three

Fluxnet sites considered here. These improvements, especially the inclusion of NSC pools also lay the groundwork for future model development and inclusion of new processes.

Acknowledgements

A. Asaadi was supported by a National Scientific and Engineering Research Council of Canada (NSERC) Visiting Postdoctoral Fellowship. We thank Fluxnet and AmeriFlux data networks for providing the data used in our study. We would also like to thank Philip Savoy for sharing LAI data for the Morgan Monroe site investigated in this study. We are also grateful to Reinel Sospedra-Alfonso and Michael Sigmond for providing comments on an earlier version of this manuscript.

References

Aboelghar, M., S. Arafat, A. Saleh, S. Naeem, M. Shirbeny, A. Belal, 2010: Retrieving leaf area index from SPOT4 satellite data Egypt. *J. Remote Sens. Space Sci.,* **13,** 121–127.

Anav, A., and Coauthors, 2013: Evaluating the land and ocean components of the global carbon cycle in the CMIP5 earth system models. *J. Climate*, **26**, 6801–6843.

Arora, V. K., 2003: Simulating energy and carbon fluxes over winter wheat using coupled land surface and terrestrial ecosystem models, *Agr. Forest Meteorol.,* **118,** 21–47.

Arora, V. K., G. J. Boer, 2003: A representation of variable root distribution in dynamic vegetation models, *Earth Interact.,* **7,** 1–19.

Arora, V. K., G. J. Boer, 2005: A parameterization of leaf phenology for the terrestrial ecosystem component of climate models. *Global Change Biology,* **11,** 39–59.

Arora, V. K., G. J. Boer, 2010: Uncertainties in the 20th century carbon budget associated with land use change, *Glob. Change Biol.,* **16,** 3327–3348.

Arora, V. K., J. F. Scinocca, G. J. Boer, J. R. Christian, K. L. Denman, G. M. Flato, V. V. Kharin, W. G. Lee, W. J. Merryfield, 2011: Carbon emission limits required to satisfy future representative concentration pathways of greenhouse gases, *Geophys. Res. Lett.,* **38,** L05805.

Arora, V. K., G. J. Boer, P. Friedlingstein, M. Eby, C. D. Jones, J. R. Christian, G. Bonan, L. Bopp, V. Brovkin, P. Cadule, T. Hajima, T. Ilyina, K. Lindsay, J. F. Tjiputra, and T. Wu, 2013: Carbon-concentration and carbon-climate feedbacks in CMIP5 earth system models. *J. Clim.* **26**, 5289–5314.

Arora, V. K., Y. Peng, W. A. Kurz, J. C. Fyfe, B. Hawkins, A. T. Werner, 2016: Potential near-future carbon uptake overcomes losses from a large insect outbreak in British Columbia, Canada. *Geophys. Res. Lett.,* **43,** 2590–2598.

604 Asner, G. P., J. M. O. Scurlock, J. A. Hicke, 2003: Global synthesis of leaf area index observations:
605 Implications for ecological and remote sensing studies. *Global Ecol. and Biogeo.,* **12,** 191–205.
606 Bao, Y., Y. Gao , S. Lü, Q. Wang, S. Zhang, J. Xu, R. Li, S. Li, D. Ma, X. Meng, H. Chen, Y. Chang,
607 2014: Evaluation of CMIP5 earth system models in reproducing leaf area index and vegetation
608 cover over the Tibetan Plateau. *J. of Meteor. Research,* **28,** 1041–1060.
609 Bazot, S., L. Barthes, D. Blanot, C. Fresneau, 2013: Distribution of non-structural nitrogen and
610 carbohydrate compounds in mature oak trees in a temperate forest at four key phenological
611 stages. Trees, 27, 1023–1034.
612 Blanken, P. D., T. A. Black, 2004: The canopy conductance of a boreal aspen forest, Prince Albert
613 National Park, Canada. *Hydrol. Process.,* **18,** 1561–1578.
614 Bonan, G. B., 2008: Forests and climate change: forcings, feedbacks, and the climate benefits of
615 forests. *Science*, **320,** 1444-1449.
616 Chatterton, N. J., K. A. Watts, K. B. Jensen, P. A. Harrison, W. H. Horton, 2006: Nonstructural
617 carbohydrates in oat forage. *J. Nutr.,* **136,** 2111S–2113S.
618 Chen, Z., L. Wang, Y. Dai, X. Wan, S. Liu, 2017: Phenology-dependent variation in the non-structural
619 carbohydrates of broadleaf evergreen species plays an important role in determining tolerance
620 to defoliation (or herbivory). Scientific Reports, 7 (10125). doi:10.1038/s41598-017-09757-2.
621 Cox, P. M., R. A. Betts, C. D. Jones, S. A. Spall, I. J. Totterdell, 2000: Acceleration of global warming
622 due to carbon-cycle feedbacks in a coupled climate model. *Nature*, **408**, 184–187.
623 Dragoni, D., H. P. Schmid, C. A. Wayson, H. Potter, C. S. B. Grimmond, J. C. Randolph, 2011:
624 Evidence of increased net ecosystem productivity associated with a longer vegetated season in a
625 deciduous forest in south-central Indiana, USA. *Global Change Biol.,* **17,** 886–897.

626 Flato, G., J. Marotzke, B. Abiodun, P. Braconnot, S. C. Chou, W. Collins, P. Cox, F. Driouech, S.
627 Emori, V. Eyring, C. Forest, P. Gleckler, E. Guilyardi, C. Jakob, V. Kattsov, C. Reason, M.
628 Rummukainen; Evaluation of Climate Models, in Climate Change 2013: The Physical Science
629 Basis. Contribution of Working Group I to the Fifth Assessment Report of the
630 Intergovernmental Panel on Climate Change, edited by: T. F. Stocker, D. Qin, G.-K. Plattner,
631 M. Tignor, S. K. Allen, J. Boschung, A. Nauels, Y. Xia, V. Bex, P. M. Midgley. Cambridge
632 Univ. Press, Cambridge, United Kingdom and New York, NY, USA, 2013, pp. 741–866.
633 Foley, J. A., I. C. Prentice, N. Ramankutty, S. Levis, D. Pollard, S. Sitch, and A. Haxeltine, 1996: An
634 integrated biosphere model of land surface processes, terrestrial carbon balance and vegetation
635 dynamics. *Global Biogeochem. Cycles*, **10,** 603–628.
636 Franklin, J., J. M. Serra-Diaz, A. D. Syphard, H. M. Regan, 2016: Global change and terrestrial plant
637 community dynamics. *Proc. Natl. Acad. Sci.*, **113,** 3725–3734.
638 Friend, A., A. Arneth , N. Kiang , M. Lomas, J. Ogee, C. Roedenbeck, S. Running, J. Santaren, S.
639 Sitch, N. Viovy, I. Woodward, S. Zaehle, 2007: Fluxnet and modelling the global carbon cycle.
640 *Global Change Biol.,* **13,** 610–633.
641 Gao, Z., H. Liu, G. G. Katul, T. Foken, 2017: Non-closure of the surface energy balance explained by
642 phase difference between vertical velocity and scalars of large atmospheric eddies. *Environ.*
643 *Res. Lett.,* **12,** p. 034025.
644 Garnaud, C., L. Sushama, and D. L. Verseghy, 2015: Impact of interactive vegetation phenology on the
645 Canadian RCM simulated climate over North America. *Climate Dyn.*, **45**, 1471–1492.
646 Gonsamo, A., J. M. Chen, 2014: Continuous observation of leaf area index at Fluxnet-Canada sites.
647 *Agric. For. Meteorol.,* **189,** 168–174.

Gough, C. M., C. E. Flower, C. S. Vogel, P. S. Curtis, 2010: Phenological and temperature controls on the temporal non-structural carbohydrate dynamics of Populus grandidentata and Quercus rubra. *Forests,* **1,** 65–81.

Hartmann, H., S. Trumbore, 2016: Understanding the roles of nonstructural carbohydrates in forest trees - from what we can measure to what we want to know. *New Phytol.,* **211,** 386–403.

Hoch, G., M. Popp, C. Körner, 2002: Altitudinal increase of mobile carbon pools in *Pinus cembra* suggest sink limitation at the Swiss treeline. *Oikos,* **98,** 361–374.

Hoch, G., A. Richter, C. Körner, 2003: Non-structural carbon compounds in temperate forest trees. *Plant Cell Environ.,* **26,** 1067–1081.

IPCC, 2013: Summary for Policymakers. In: Climate Change 2013: The Physical Science Basis. Contribution of Working Group I to the Fifth Assessment Report of the Intergovernmental Panel on Climate Change [Stocker, T.F., D. Qin, G.-K. Plattner, M. Tignor, S. K. Allen, J. Boschung, A. Nauels, Y. Xia, V. Bex and P.M. Midgley (eds.)]. Cambridge University Press, Cambridge, United Kingdom and New York, NY, USA.

Kattge, J., W. Knorr, T. Raddatz, and C. Wirth, 2009: Quantifying photosynthetic capacity and its relationship to leaf nitrogen content for global-scale terrestrial biosphere models. *Global Change Biology,* **15,** 976–991.

Kikuzawa, K., 1995: Leaf phenology as an optimal strategy for carbon gain in plants. *Can. J. Bot.,* **73,** 158–163.

Klein, T., Y. Vitasse, G. Hoch, 2016: Coordination between growth, phenology and carbon storage in three coexisting deciduous tree species in a temperate forest. *Tree Physiology,* **36,** 847–855.

Knyazikhin, Y., J. V. Martonchik, D. J. Diner, R. B. Myneni, M. Verstraete, B. Pinty, and N. Gobron, 1998: Estimation of vegetation canopy leaf area index and fraction of absorbed

photosynthetically active radiation from atmosphere-corrected MISR data, *J. Geophys. Res.,* **103,** 32239–32256.

Kozlowski, T. T., 1992: Carbohydrate sources and sinks in woody plants. *Bot. Rev.,* **58,** 107–222.

Kucharik C. J., C. C. Barford, M. E. Maayar, S. C. Wofsy, R. K. Monson, D. D. Baldocchi, 2006: A multiyear evaluation of a dynamic global vegetation model at three ameriflux forest sites: vegetation structure, phenology, soil temperature, and CO2 and H2O vapor exchange. *Ecological Modelling* **196**, 1–31.

Le Quéré, C., and Coauthors, 2016: Global Carbon Budget 2016, *Earth Syst. Sci. Data,* **8,** 605-649.

Le Quéré, C., and Coauthors, 2017: Global Carbon Budget 2017, *Earth Syst. Sci. Data Discuss.,* in review.

Levis, S., G. B. Bonan, 2004: Simulating springtime temperature patterns in the community atmosphere model coupled to the community land model using prognostic leaf area. *J. Clim.,* **17,** 4531–4540.

Li, M. H., G. Hoch, C. Körner, 2001: Spatial variability of mobile carbohydrates within Pinus cembra trees at the alpine treeline. *Phyton,* **41,** 203–213.

Li, N., N. He, G. Yu, Q. Wang, J. Sun, 2016: Leaf non-structural carbohydrates regulated by plant functional groups and climate: evidences from a tropical to cold-temperate forest transect. *Ecological Indicators,* **62,** 22–31.

Mäkelä, A., J. Landsberg, A. R. Ek, T. E. Burk, M. Ter-Mikaelian, G. I. Ågren, C. D. Oliver, P. Puttonen, 2000: Process-based models for forest ecosystem management: current state of the art and challenges for practical implementation. *Tree Physiology,* **20,** 289–298.

Mei, L., Y. Xiong, J. Gu, Z. Wang, D. Guo, 2015: Whole-tree dynamics of non-structural carbohydrate and nitrogen pools across different seasons and in response to girdling in two temperate trees. *Oecologia,* **177,** 333–344.

695 Melton, J. R., V. K. Arora, 2014: Sub-grid scale representation of vegetation in global land surface
696 schemes: implications for estimation of the terrestrial carbon sink. *Biogeosciences,* **11,** 1021–
697 1036.
698 Melton, J. R., R. K. Shrestha, and V. K. Arora, 2015: The influence of soils on heterotrophic
699 respiration exerts a strong control on net ecosystem productivity in seasonally dry Amazonian
700 forests. *Biogeosciences,* **12,** 1151–1168.
701 Melton, J. R., V. K. Arora, 2016: Competition between plant functional types in the Canadian
702 Terrestrial Ecosystem Model (CTEM) v. 2.0, *Geosci. Model Dev.,* **9,** 323–361.
703 Menzel, A., and Coauthors, 2006: European phenological response to climate change matches the
704 warming pattern. *Global Change Biol,* **12,** 1969–1976.
705 Mitchell P. J., A. P. O'Grady, D. T. Tissue, D. A. White, M. L. Ottenschlaeger, E. A. Pinkard, 2013:
706 Drought response strategies define the relative contributions of hydraulic dysfunction and
707 carbohydrate depletion during tree mortality. *New Phytologist,* **197,** 862–872.
708 Moore, K. E., and Coauthors, 1996: Seasonal variation in radiative and turbulent exchange at a
709 deciduous forest in central Massachusetts. *J. Appl. Meteorol.,* **35,** 122–134.
710 Myneni, R. B., C. D. Keeling, C. J. Tucker, G. Asrar, R. R. Nemani, 1997: Increased plant growth in
711 the northern high latitudes from 1981 to 1991. *Nature,* **386,** 698–702.
712 Myneni, R. B., J. Dong, C. J. Tucker, R. K. Kaufmann, P. E. Kauppi, J. Liski, L. Zhou, V. Alexeyev,
713 and M. K. Hughes, 2001: A large carbon sink in the woody biomass of Northern forests. *Proc.*
714 *Natl. Acad. Sci.,* **98,** 14784-14789.
715 Norby, R. J., J. D. Sholtis, C. A. Gunderson, S. S. Jawdy, 2003: Leaf dynamics of a deciduous forest
716 canopy: no response to elevated CO2. *Oecologia,* **136,** 574–584.

717 Oberhuber, W., I. Swidrak, D. Pirkebner, A. Gruber, 2011: Temporal dynamics of nonstructural
718 carbohydrates and xylem growth in Pinus sylvestris exposed to drought. *Canadien Journal of*
719 *Forest Research,* **41,** 1590–1597.
720 O'Brien, M. J., S. Leuzinger, C. D. Philipson, J. Tay, A. Hector, 2014: Drought survival of tropical tree
721 seedlings enhanced by non-structural carbohydrate levels. *Nature Climate Change,* **4,** 710–714.
722 Ögren, E., 2000: Maintenance respiration correlates with sugar but not nitrogen concentration in
723 dormant plants. *Physiol. Plant.,* **108,** 295–299.
724 Oliphant, A. J., C. S. B. Grimmond, H. N. Zutter, H. P. Schmid, H.-B. Su, S. L. Scott, B. Offerle, J. C.
725 Randolph, J. Ehman. 2004: Heat storage and energy balance fluxes for a temperate deciduous
726 forest. *Agric. For. Meteorol.,* **126,** 185-201.
727 Palacio, S., P. Millard, M. Maestro, G. Montserrat-Marti, 2007: Non-structural carbohydrates and
728 nitrogen dynamics in Mediterranean sub-shrubs: an analysis of the functional role of over
729 wintering leaves. *Plant Biol.,* **9,** 49–58.
730 Parmesan, C., 2006: Ecological and evolutionary responses to recent climate change. *Annual Review of*
731 Ecology, Evolution and Systematics, **37,** 637–669.
732 Peng, Y., V. K. Arora, W. A. Kurz, R. A. Hember, B. J. Hawkins, J. C. Fyfe, and A. T. Werner, 2014:
733 Climate and atmospheric drivers of historical terrestrial carbon uptake in the province of British
734 Columbia, Canada, *Biogeosciences,* **11,** 635-649.
735 Pilegaard, K., T. N. Mikkelsen, C. Beier, N. O. Jensen, P. Ambus, H. Ro-Poulsen, 2003: Field
736 measurements of atmosphere-biosphere interactions in a Danish beech forest. *Boreal*
737 *Environment Research,* **8,** 315–333.
738 Poorter, L., K. Kitajima, 2007: Carbohydrate storage and light requirements of tropical moist and dry
739 forest tree species. *Ecology,* **88,** 1000–1011.

740 Prentice, I.C., G.D. Farquhar, M.J.R. Fasham, M.L. Goulden, M. Heimann, V.J. Jaramillo, H.S.
741 Kheshgi, C. Le Quéré, R.J. Scholes, D.W.R. Wallace, D. Archer, M.R. Ashmore, O. Aumont,
742 D. Baker, M. Battle, M. Bender, L.P. Bopp, P. Bousquet, K. Caldeira, P. Ciais, P.M. Cox, W.
743 Cramer, F. Dentener, I.G. Enting, C.B. Field, P. Friedlingstein, E.A. Holland, R.A. Houghton,
744 J.I. House, A. Ishida, A.K. Jain, I.A. Janssens, F. Joos, T. Kaminski, C.D. Keeling, R.F.
745 Keeling, D.W. Kicklighter, K.E. Kohfeld, W. Knorr, R. Law, T. Lenton, K. Lindsay, E. Maier-
746 Reimer, A.C. Manning, R.J. Matear, A.D. McGuire, J.M. Melillo, R. Meyer, M. Mund, J.C.
747 Orr, S. Piper, K. Plattner, P.J. Rayner, S. Sitch, R. Slater, S. Taguchi, P.P. Tans, H.Q. Tian,
748 M.F. Weirig, T. Whorf, A. Yool, L. Pitelka, A. Ramirez Rojas, 2001: The Carbon Cycle and
749 Atmopsheric Carbon Dioxide. In: Climate Change 2001: The Scientific Basis. Contribution of
750 Working Group I to the Third Assessment Report of the Intergovernmental Panel on Climate
751 Change [Houghton, J.T., Y. Ding, D.J. Griggs, M. Noguer, P.J. van der Linden, X. Dai, K.
752 Maskell, and C.A. Johnson (eds.)]. Cambridge University Press, Cambridge, United Kingdom
753 and New York, NY, USA, 881pp.

754 Richardson, A. D., and Coauthors, 2010: Influence of spring and autumn phenological transitions on
755 forest ecosystem productivity. *Philos. Trans. R. Soc. B,* **365,** 3227–3246.

756 Richardson, A. D., and Coauthors, 2012: Terrestrial biosphere models need better representation of
757 vegetation phenology: results from the North American Carbon Program Site Synthesis. *Global*
758 *Change Biol.,* **18,** 566–584.

759 Richardson, A. D., M. S. Carbone, T. F. Keenan, C. I. Czimczik, D. Y. Hollinger, P. Murakami, P. G.
760 Schaberg, X. Xu, 2013: Seasonal dynamics and age of stemwood nonstructural carbohydrates in
761 temperate forest trees. *New Phytologist,* **197,** 850–861.

762 Rosas, T., L. Galiano, R. Ogaya, J. Peñuelas, J. Martínez-Vilalta, 2013: Dynamics of non-structural
763 carbohydrates in three Mediterranean woody species following long-term experimental drought.
764 *Frontiers in Plant Science,* **4,** 1–16.
765 Running, S., D. Baldocchi, D. Turner, S. Gower, P. Bakwin, K. Hibbard, 1999: A global terrestrial
766 monitoring network integrating tower fluxes, flask sampling, ecosystem modelling and EOS
767 satellite data. *Remote Sens. Environ.,* **70,** 108–127.
768 Ryu, S. R., J. Chen, A. Noormets, M. K. Bresee, S. V. Ollinger, 2008: Comparisons between PnET-
769 Day and eddy covariance based gross ecosystem production in two Northern Wisconsin forests.
770 *Agric. For. Meteorol.,* **148,** 247–256.
771 Saffell, B. J., F. C. Meinzer, D. R. Woodruff, D. C. Shaw, S. L. Voelker, B. Lachenbruch, K. Falk,
772 2014: Seasonal carbohydrate dynamics and growth in Douglas-fir trees experiencing chronic,
773 fungal-mediated reduction in functional leaf area. *Tree Physiol.,* **34,** 218–228.
774 Sakai, R. K., D. R. Fitzjarrald, K. E. Moore, 1997: Detecting leaf area and surface resistance during
775 transition seasons. *Agric. For. Meteorol.,* **84,** 273–284.
776 Sato, H., A. Ito, A. Ito, T. Ise, E. Kato, 2015: Current status and future of land surface models. *Soil Sci.*
777 *Plant Nutr.*, **61,** 34–47.
778 Savoy, P., D. S. Mackay, 2015: Modeling the seasonal dynamics of leaf area index based on
779 environmental constraints to canopy development. *Agric. For. Meteorol.,* **200,** 46–56.
780 Sitch, S., C. Huntingford, N. Gedney, P. E. Levy, M. Lomas, S. L. Piao, R. Betts, P. Ciais, P. Cox, P.
781 Friedlingstein. C. D. Jones, I. C. Prentice, F. I. Woodward, 2008: Evaluation of the terrestrial
782 carbon cycle, future plant geography and climate-carbon cycle feedbacks using five Dynamic
783 Global Vegetation Models (DGVMs). *Glob. Change Biol.,* **14,** 2015-2039.

784 Smith, L. M., S. Hall, 2016: Extended leaf phenology may drive plant invasion through direct and
785 apparent competition. *Oikos,* **125,** 839–848.
786 Sperling, O., J. M. Earles, F. Secchi, J. Godfrey, M. A. Zwieniecki, 2015: Frost induces respiration and
787 accelerates carbon depletion in trees. *PLoS One,* 10:e0144124.
788 Sperling, O., L. C. R. Silva, A. Tixier, G. Théroux-Rancourt, M. A. Zwieniecki, 2017: Temperature
789 gradients assist carbohydrate allocation within trees. *Sci. Rep.,* **7** (3265). doi:10.1038/s41598-
790 017-03608-w
791 Teixeira, E. I., D. J. Mott, M. V. Mickelbart, 2007: Seasonal patterns of root C and N reserves of
792 lucerne crops (Medicago sativa L.) grown in a temperate climate were affected by defoliation
793 regime. *Eur J Agron,* **26,** 10–20.
794 Verseghy, D., 2012: CLASS – the Canadian Land Surface Scheme (Version 3.6), Technical
795 Documentation, Tech. rep., Science and Technology Branch, Environment Canada.
796 Würth, M. K. R., S. Peláez-Riedl, S. J. Wright, C. Körner, 2005: Non-structural carbohydrate pools in a
797 tropical forest. *Oecologia,* **143,** 11–24.
798 Wyka, T. P., P. Karolewski, R. Żytkowiak, P. Chmielarz, J. Oleksyn, 2016: Whole-plant allocation to
799 storage and defense in juveniles of related evergreen and deciduous shrub species. *Tree*
800 *Physiology,* **36,** 536–547.
801 Xavier, A. C., and C. A. Vettorazzi, 2004: Mapping leaf area index through spectral vegetation indices
802 in a subtropical watershed. International J. of Remote Sensing, 25, 1661–1672.
803 Xie, Y., X. Wang, and J. A. Silander, 2015: Deciduous forest responses to temperature, precipitation,
804 and drought imply complex climate change impacts. *Proc. Natl. Acad. Sci.,* **112,** 13585–13590.
805 Zhu, W. Z., M. Cao, S. G. Wang, W. F. Xiao, M. H. Li, 2012: Seasonal dynamics of mobile carbon
806 supply in Quercus aquifolioides at the upper elevational limit. *PLoS ONE,* **7,** e34213.

807 Zobler, L., 1986: A world soil file for global climate modelling. NASA Technical Memorandum
808 87802. NASA Goddard Institute for Space Studies, New York, New York, U.S.A.
809 Zotz, G., A. Richter, 2006: Changes in carbohydrate and nutrient contents throughout a reproductive
810 cycle indicate that phosphorus is a limiting nutrient in the epiphytic bromeliad. *Werauhia*
811 *sanguinolenta. Ann. Bot.,* **97,** 745–754.
812
813

Biogeosciences Discuss., https://doi.org/10.5194/bg-2018-168
Manuscript under review for journal Biogeosciences
Discussion started: 14 May 2018

List of Tables

Table 1. Plant functional types (PFTs) represented in CTEM and their relation to CLASS PFTs.

Table 2. Fluxnet site locations, characteristics, and years of data availability.

Table 3. Simulated and observation-based turbulent energy and carbon fluxes, and LAI at the three Fluxnet sites. The driving shortwave and longwave radiation are also shown.

Biogeosciences Discuss., https://doi.org/10.5194/bg-2018-168
Manuscript under review for journal Biogeosciences
Discussion started: 14 May 2018

Table 1: Plant functional types (PFTs) represented in CTEM and their relation to CLASS PFTs.

CLASS PFTs	CTEM PFTs
Needleleaf trees	Needleleaf Evergreen trees
	Needleleaf Deciduous trees
Broadleaf trees	Broadleaf Evergreen trees
	Broadleaf Cold Deciduous trees
	Broadleaf Drought/Dry Deciduous trees
Crops	C3 Crops
	C4 Crops
Grasses	C3 Grasses
	C4 Grasses

Biogeosciences Discuss., https://doi.org/10.5194/bg-2018-168
Manuscript under review for journal Biogeosciences
Discussion started: 14 May 2018

Table 2. Fluxnet site locations, characteristics, and years of data availability

Site Name	Harvard forest (US-Ha1)	Morgan Monroe state forest (US-MMS)	Uni. of Mich. Biological station (US-UMB)
Lat, Lon,Elevation	42.53º, -72.17º, 340m	39.32º, -86.41º, 275m	45.55º, -84.71º, 234m
Biome Type	Broadleaf deciduous forest	Broadleaf deciduous forest	Broadleaf deciduous forest
Species	Red Oak (Quercus rubra), Red Maple (Acer rubrum), Hemlock (Tsuga canadensis), White Pine (Pinus strobus)	Maple-beech (Fagus grandifolia), Oak-Hickory	Conifer understory, Aspen (Populus tremuloides), Hemlock (Cicuta), and other northern hardwood trees
Mean annual air T (ºC)	8.2	12.4	7.2
Mean annual precip. (mm)	1189	1083	613
Mean annual SW Radiation (W/m^2)	151	167	154
Mean annual LW Radiation (W/m^2)	263	329	299
Soil depth (m)	2.5	2.5	2.6
% of soil sand (layer 1, 2, 3)	68.5, 66.5, 72.25	21, 22.5, 30.25	71, 72.5, 73.25
% of soil clay (layer 1, 2, 3)	5, 5, 4.25	21, 23, 23.75	7, 7, 7.75
Years for which LAI data are available	1998-2013	1999-2006	1997-2013

Biogeosciences Discuss., https://doi.org/10.5194/bg-2018-168
Manuscript under review for journal Biogeosciences
Discussion started: 14 May 2018

Table 3. Simulated and observation-based turbulent energy and carbon fluxes, and LAI at the three Fluxnet sites. The driving shortwave and longwave radiation are also shown.

Site name		Harvard forest (US-Ha1)	Morgan Monroe (US-MMS)	Uni. of Mich. (US-UMB)
Land -atmosphere CO_2 fluxes (gC m^{-2} yr^{-1}) and LAI (m^2/m^2)				
Gross primary productivity	Observed	3.9	4.5	3.6
	CLASS-CTEM original	3.6	5.0	3.6
	CLASS-CTEM modified	3.7	5.3	3.7
Ecosystem respiration	Observed	3.3	3.3	2.9
	CLASS-CTEM original	3.6	4.9	3.5
	CLASS-CTEM modified	3.7	5.3	3.7
Net ecosystem productivity	Observed	0.7	1.2	0.7
	CLASS-CTEM original	0.02	0.1	0.0
	CLASS-CTEM modified	0.0	0.0	0.0
Leaf area index	Observed	1.8	3.0	2.8
	CLASS-CTEM original	2.0	3.1	1.9
	CLASS-CTEM modified	1.9	3.0	1.8
Energy fluxes and energy budget (W/m^2)				
Net radiation (R_n)	observed	78.9	89.6	78.1
	CLASS-CTEM original	59.6	89.2	66.8
	CLASS-CTEM modified	59.6	89.6	67.2
Latent heat flux (LE)	observed	34.0	38.3	35.4
	CLASS-CTEM original	38.9	68.6	47.9
	CLASS-CTEM modified	39.4	69.3	48.3
Sensible heat flux (H)	observed	29.3	25.1	29.4
	CLASS-CTEM original	20.7	20.6	18.9
	CLASS-CTEM modified	20.2	20.3	18.9
R_n-LE-H	observed	15.6	26.2	13.3
	CLASS-CTEM original	0	0	0
	CLASS-CTEM modified	0	0	0

Biogeosciences Discuss., https://doi.org/10.5194/bg-2018-168
Manuscript under review for journal Biogeosciences
Discussion started: 14 May 2018

List of Figures

1 Schematic representation of the CTEM model after adding non-structural carbohydrate pools. The arrows in blue color show the new non-structural carbohydrate fluxes as shown in Eqs. (5-6).

2 Latitude dependence factor (Γ) (equation 8) for reducing allocation fraction to leaves after summer solstice.

3 Location of the three Fluxnet sites chosen in this study to evaluate the changes made to the CLASS-CTEM parameterizations aimed to improve leaf phenology.

4 Observed and CLASS-CTEM simulated daily a) LAI (m^2/m^2), b) GPP ($g.C/m^2.day$), c) NEP ($g.C/m^2.day$), and d) Ecosystem respiration ($g.C/m^2.day$) for US-Ha1 (Harvard Forest) Fluxnet site.

5 Observed and CLASS-CTEM simulated daily a) LAI (m^2/m^2), b) GPP ($g.C/m^2.day$), c) NEP ($g.C/m^2.day$), and d) Ecosystem respiration ($g.C/m^2.day$) for US-MMS (Morgan Monroe State Forest) Fluxnet site.

6 Observed and CLASS-CTEM simulated daily a) LAI (m^2/m^2), b) GPP ($g.C/m^2.day$), c) NEP ($g.C/m^2.day$), and d) Ecosystem respiration ($g.C/m^2.day$) for US-UMB (University of Michigan Biological Reserve) Fluxnet site.

7 CLASS-CTEM (modified version) simulated values of total (panel a) and non-structural (panel c) carbohydarte pools ($kg.C/m^2$). Panel (b) shows the reallocation of carbon from non-structural stem and root pools to leaves during leaf onset in spring and panel (d) shows the carbon flux from non-structural to structural pools for leaf, stem and root components ($gC/m^2.day$) for US-Ha1(Harvard Forest) Fluxnet site. The plots show mean daily values across all years for which the meteorological data were available after the model pools reached equilibrium.

Biogeosciences Discuss., https://doi.org/10.5194/bg-2018-168
Manuscript under review for journal Biogeosciences
Discussion started: 14 May 2018

8 CLASS-CTEM (modified version) simulated values of total (panel a) and non-structural (panel c) carbohydarte pools (kg.C/m^2). Panel (b) shows the reallocation of carbon from non-structural stem and root pools to leaves during leaf onset in spring and panel (d) shows the carbon flux from non-structural to structural pools for leaf, stem and root components (g.C/m^2.day) for US-MMS (Morgan Monroe State Forest) Fluxnet site. The plots show mean daily values across all years for which the meteorological data were available after the model pools reached equilibrium.

9 CLASS-CTEM (modified version) simulated values of total (panel a) and non-structural (panel c) carbohydarte pools (kg.C/m^2). Panel (b) shows the reallocation of carbon from non-structural stem and root pools to leaves during leaf onset in spring and panel (d) shows the carbon flux from non-structural to structural pools for leaf, stem and root components (g.C/m^2.day) for US-UMB (University of Michigan Biological Reserve) Fluxnet site. The plots show mean daily values across all years for which the meteorological data were available after the model pools reached equilibrium.

10 Observed and CLASS-CTEM simulated daily net radiation (W/m^2), latent heat flux (W/m^2), and sensible heat flux (W/m^2) for the three Fluxnet sites.

Biogeosciences Discuss., https://doi.org/10.5194/bg-2018-168
Manuscript under review for journal Biogeosciences
Discussion started: 14 May 2018

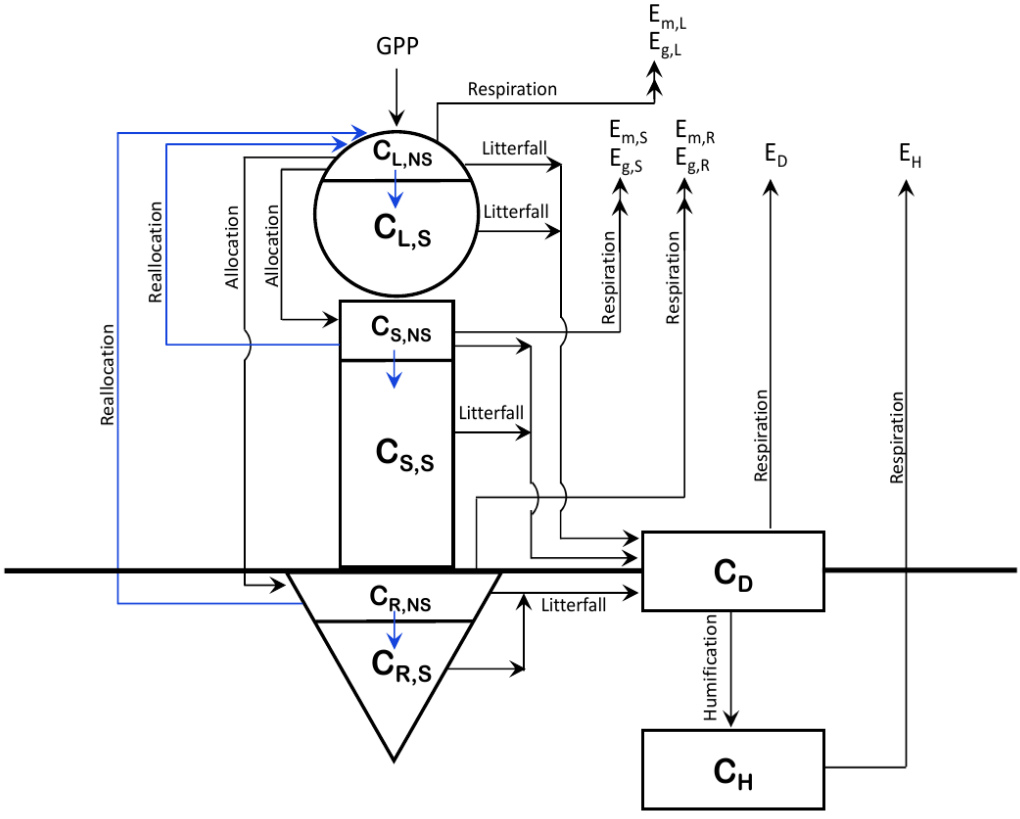

Figure 1: Schematic representation of the CTEM model after adding non-structural carbohydrate pools. The arrows in blue color show the new non-structural carbohydrate fluxes as shown in Eqs. (5-6).

Biogeosciences Discuss., https://doi.org/10.5194/bg-2018-168
Manuscript under review for journal Biogeosciences
Discussion started: 14 May 2018

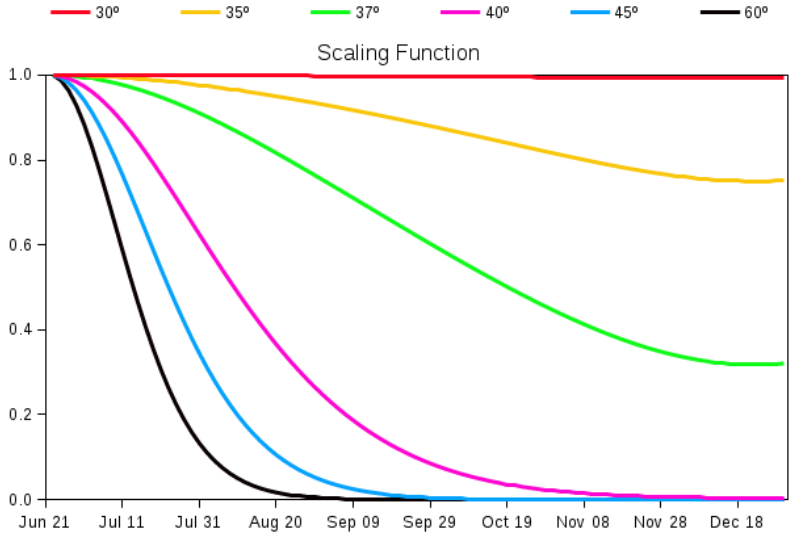

Figure 2: Latitude dependence factor (Γ) (Eq. 8) for reducing allocation fraction to leaves after summer solstice.

Biogeosciences Discuss., https://doi.org/10.5194/bg-2018-168
Manuscript under review for journal Biogeosciences
Discussion started: 14 May 2018

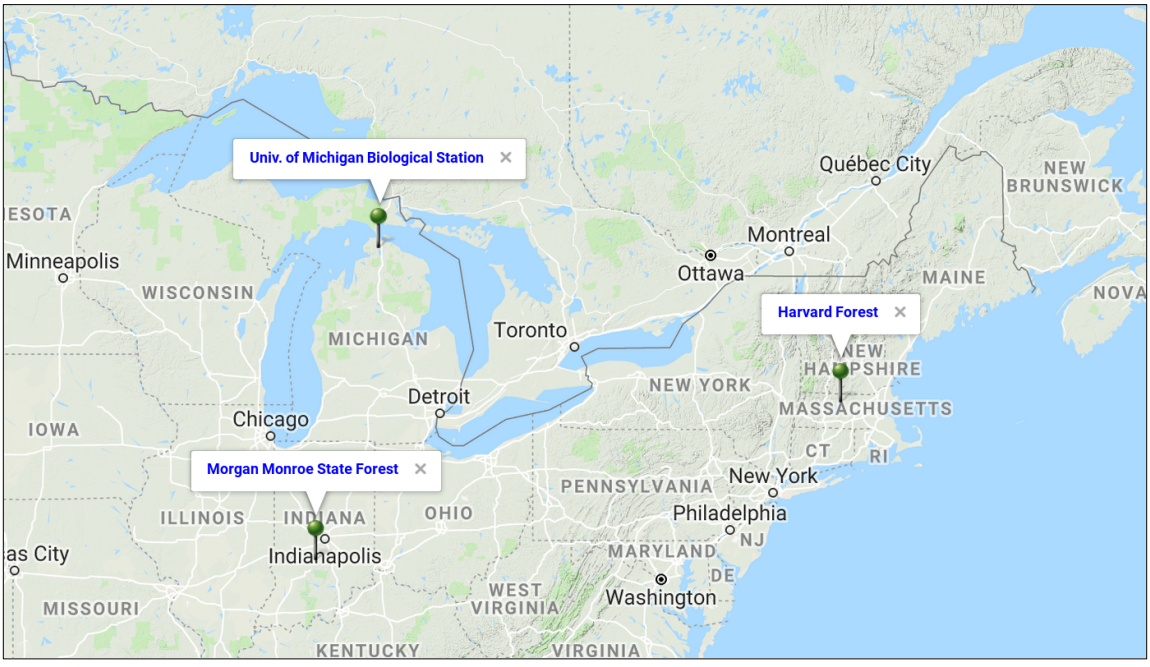

Figure 3: Location of the three Fluxnet sites chosen in this study to evaluate the changes made to the CLASS-CTEM parameterizations aimed to improve leaf phenology. Figure adapted from Google maps.

Biogeosciences Discuss., https://doi.org/10.5194/bg-2018-168
Manuscript under review for journal Biogeosciences
Discussion started: 14 May 2018

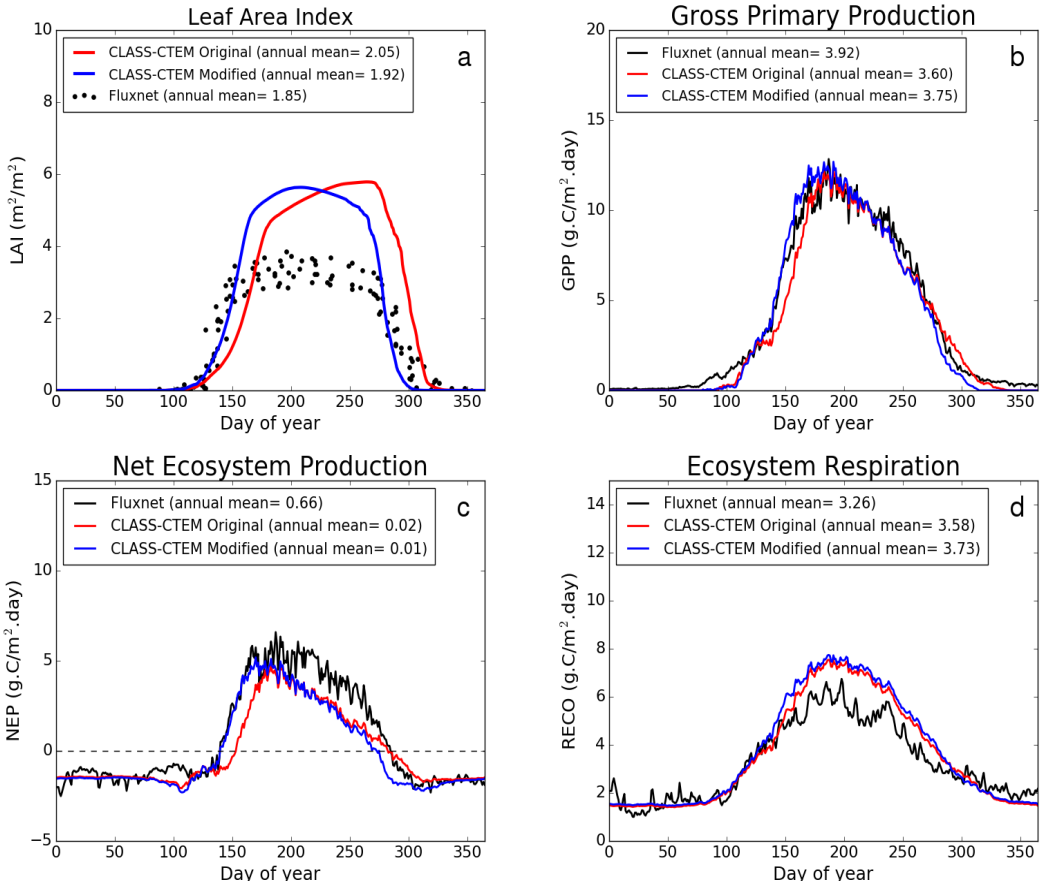

Figure 4: Observed and CLASS-CTEM simulated daily a) LAI (m^2/m^2), b) GPP ($g.C/m^2.day$), c) NEP ($g.C/m^2.day$), and d) Ecosystem respiration ($g.C/m^2.day$) for US-Ha1 (Harvard Forest) Fluxnet site.

Biogeosciences Discuss., https://doi.org/10.5194/bg-2018-168
Manuscript under review for journal Biogeosciences
Discussion started: 14 May 2018

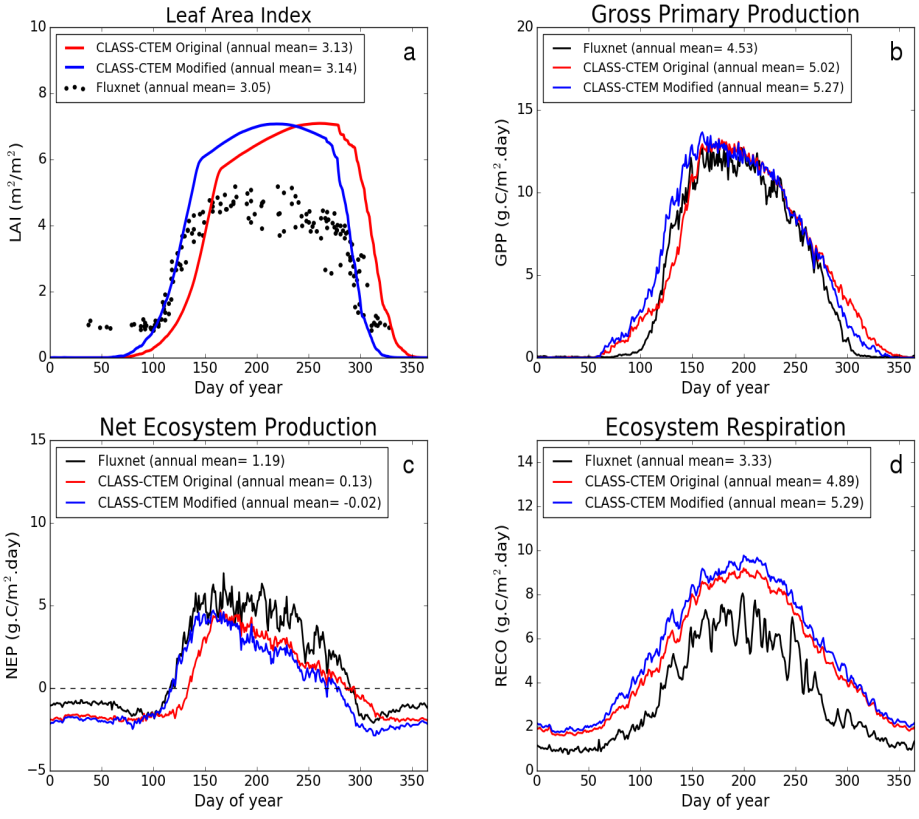

Figure 5: Observed and CLASS-CTEM simulated daily a) LAI (m^2/m^2), b) GPP ($g.C/m^2.day$), c) NEP ($g.C/m^2.day$), and d) Ecosystem respiration ($g.C/m^2.day$) for US-MMS (Morgan Monroe State Forest) Fluxnet site.

Biogeosciences Discuss., https://doi.org/10.5194/bg-2018-168
Manuscript under review for journal Biogeosciences
Discussion started: 14 May 2018

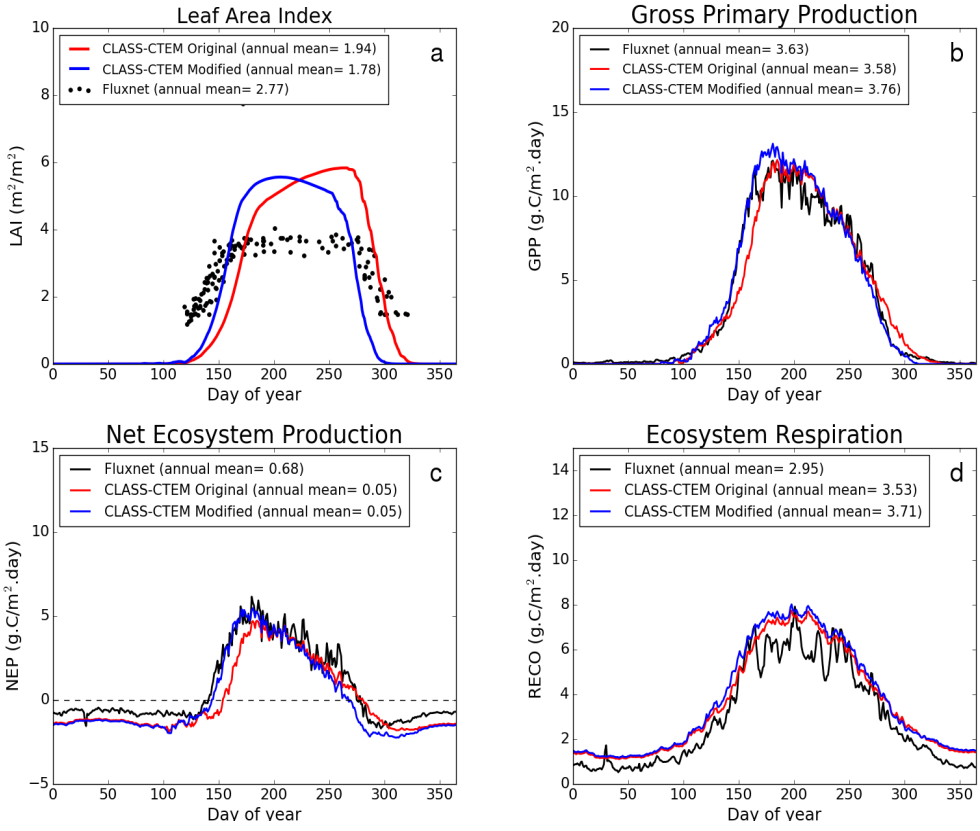

Figure 6: Observed and CLASS-CTEM simulated daily a) LAI (m^2/m^2), b) GPP ($g.C/m^2.day$), c) NEP ($g.C/m^2.day$), and d) Ecosystem respiration ($g.C/m^2.day$) for US-UMB (University of Michigan Biological Reserve) Fluxnet site.

Biogeosciences Discuss., https://doi.org/10.5194/bg-2018-168
Manuscript under review for journal Biogeosciences
Discussion started: 14 May 2018

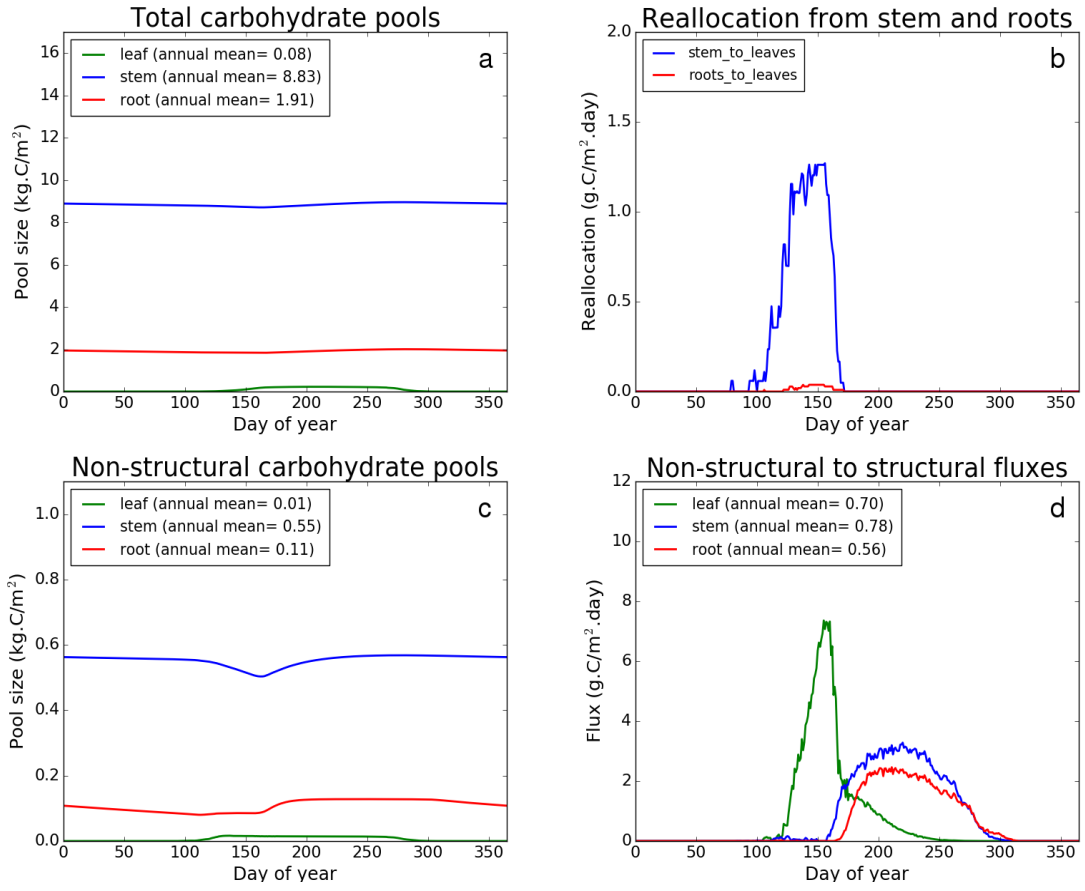

Figure 7: CLASS-CTEM (modified version) simulated values of total (panel a) and non-structural (panel c) carbohydarte pools (kg.C/m^2). Panel (b) shows the reallocation of carbon from non-structural stem and root pools to leaves during leaf onset in spring and panel (d) shows the carbon flux from non-structural to structural pools for leaf, stem and root components (gC/m^2.day) for US-Ha1(Harvard Forest) Fluxnet site. The plots show mean daily values across all years for which the meteorological data were available after the model pools reached equilibrium.

Biogeosciences Discuss., https://doi.org/10.5194/bg-2018-168
Manuscript under review for journal Biogeosciences
Discussion started: 14 May 2018

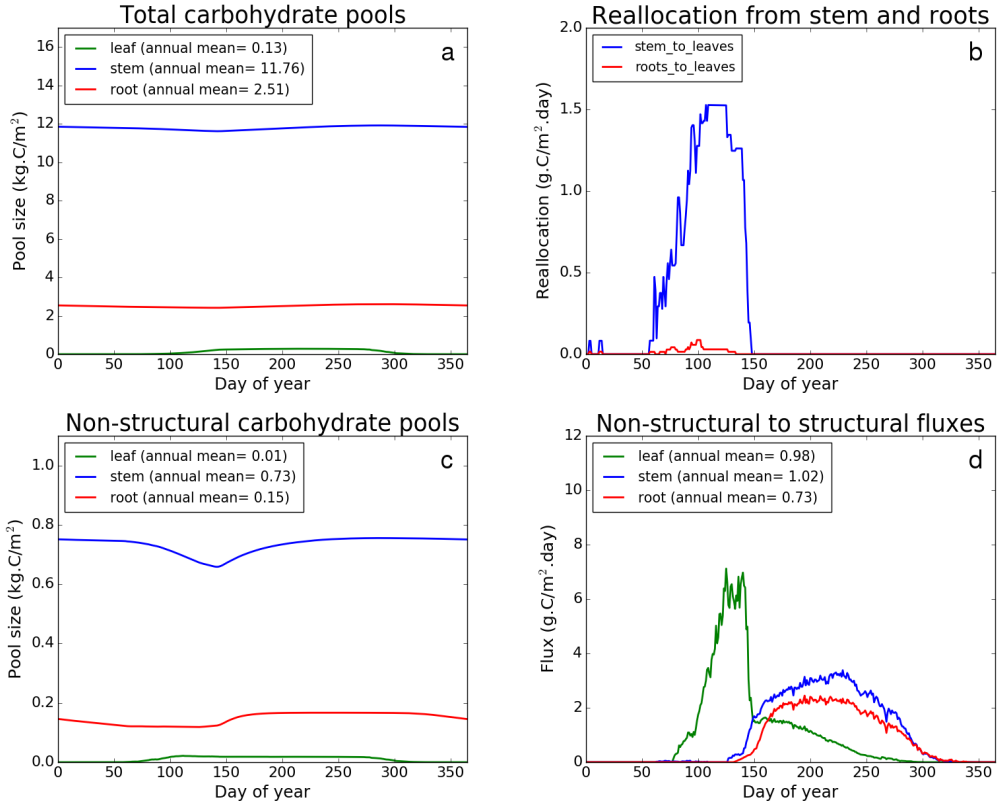

Figure 8: CLASS-CTEM (modified version) simulated values of total (panel a) and non-structural (panel c) carbohydarte pools (kg.C/m^2). Panel (b) shows the reallocation of carbon from non-structural stem and root pools to leaves during leaf onset in spring and panel (d) shows the carbon flux from non-structural to structural pools for leaf, stem and root components (g.C/m^2.day) for US-MMS (Morgan Monroe State Forest) Fluxnet site. The plots show mean daily values across all years for which the meteorological data were available after the model pools reached equilibrium.

Biogeosciences Discuss., https://doi.org/10.5194/bg-2018-168
Manuscript under review for journal Biogeosciences
Discussion started: 14 May 2018

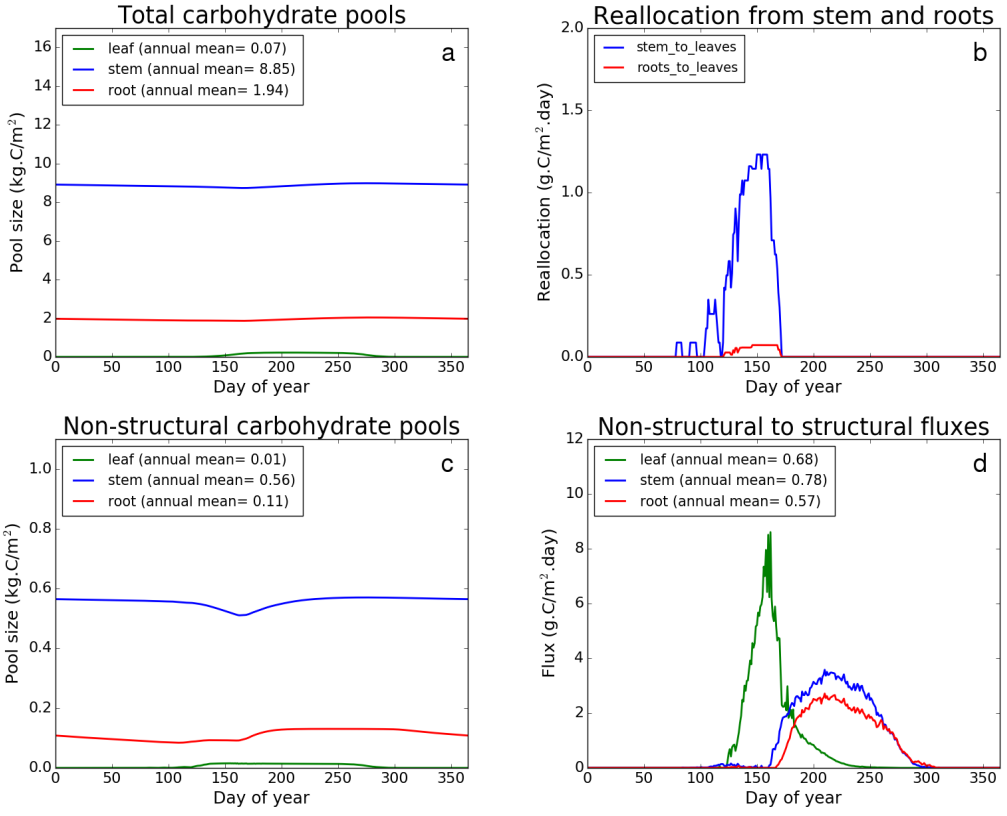

Figure 9: CLASS-CTEM (modified version) simulated values of total (panel a) and non-structural (panel c) carbohydarte pools (kg.C/m^2). Panel (b) shows the reallocation of carbon from non-structural stem and root pools to leaves during leaf onset in spring and panel (d) shows the carbon flux from non-structural to structural pools for leaf, stem and root components (g.C/m^2.day) for US-UMB (University of Michigan Biological Reserve) Fluxnet site. The plots show mean daily values across all years for which the meteorological data were available after the model pools reached equilibrium.

Biogeosciences Discuss., https://doi.org/10.5194/bg-2018-168
Manuscript under review for journal Biogeosciences
Discussion started: 14 May 2018

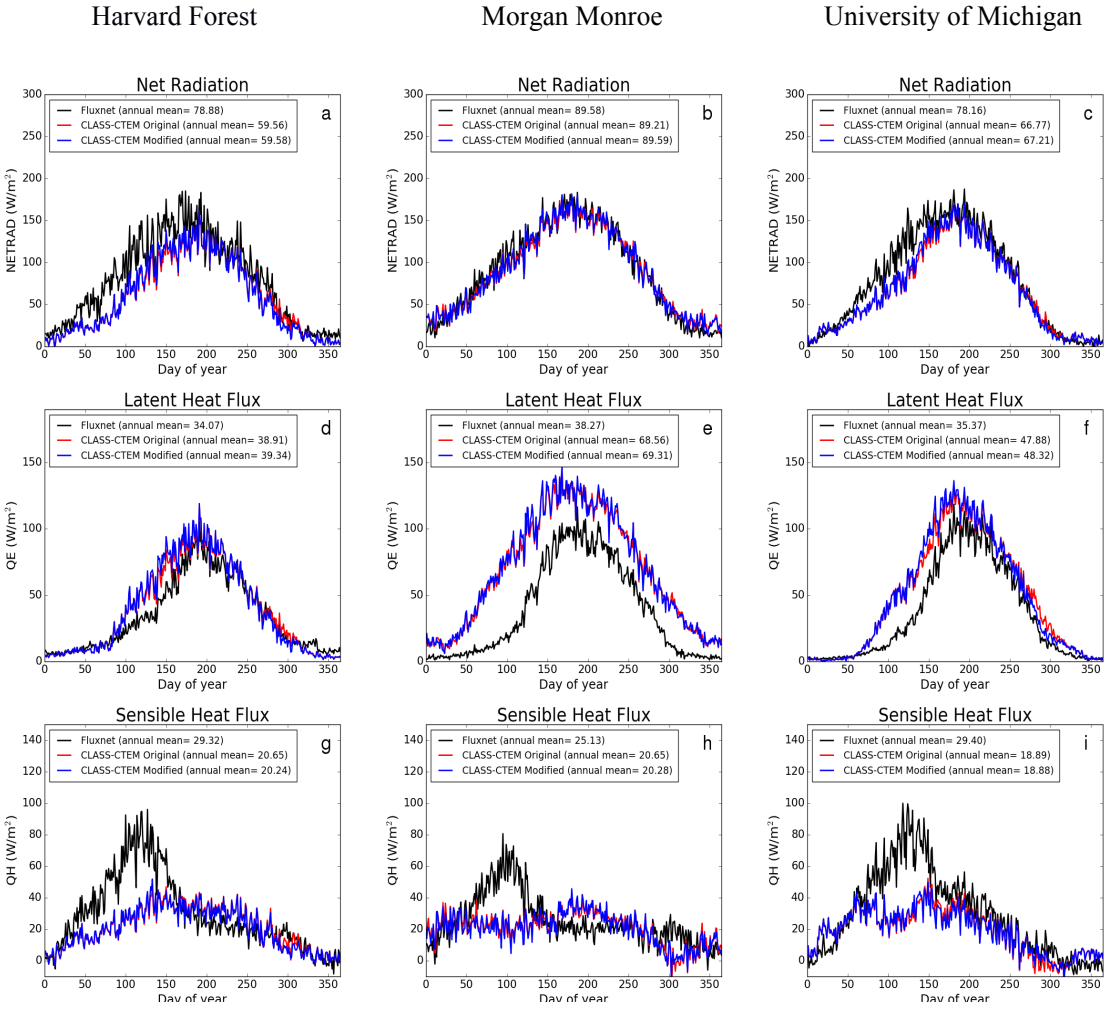

Figure 10: Observed and CLASS-CTEM simulated daily net radiation (W/m^2), latent heat flux (W/m^2), and sensible heat flux (W/m^2) for the three Fluxnet sites.